8-9-2016

Autophagic Turnover of Inactive 26S Proteasomes in Yeast Is Directed by the Ubiquitin Receptor Cue5 and the Hsp42 Chaperone

Richard S. Marshall

Fionn McLoughlin

Richard D. Vierstra
Washington University in St Louis, rdvierstra@wustl.edu

Article

Cell Reports

Autophagic Turnover of Inactive 26S Proteasomes in Yeast Is Directed by the Ubiquitin Receptor Cue5 and the Hsp42 Chaperone

Graphical Abstract

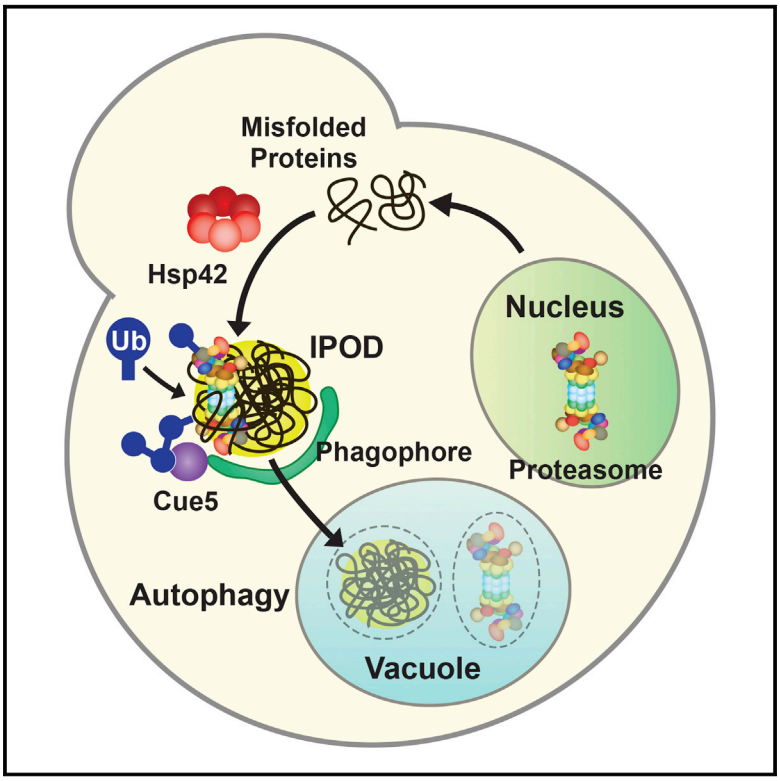

Authors

Richard S. Marshall, Fionn McLoughlin, Richard D. Vierstra

Correspondence

rdvierstra@wustl.edu

In Brief

Marshall et al. find that 26S proteasomes are degraded by autophagy in yeast, a process stimulated by inactivation or nitrogen starvation. Proteasome inhibition is accompanied by both Hsp42-mediated aggregation and ubiquitylation of the complex, which is then targeted to autophagic membranes by the ubiquitin binding autophagy receptor Cue5.

Highlights

- The yeast 26S proteasome is degraded by Atg8-mediated autophagy
- Nitrogen starvation and inactivation stimulate proteaphagy via distinct pathways
- Proteasome inhibition is accompanied by extensive ubiquitylation of the complex
- Proteaphagy engages the Cue5 autophagy receptor and the Hsp42 chaperone

Marshall et al., 2016, Cell Reports *16*, 1717–1732
August 9, 2016
http://dx.doi.org/10.1016/j.celrep.2016.07.015

Cell Reports
Article

OPEN ACCESS
CellPress

Autophagic Turnover of Inactive 26S Proteasomes in Yeast Is Directed by the Ubiquitin Receptor Cue5 and the Hsp42 Chaperone

Richard S. Marshall,[1,2] Fionn McLoughlin,[2] and Richard D. Vierstra[1,2,*]
[1]Department of Genetics, University of Wisconsin, 425 Henry Mall, Madison, WI 53706, USA
[2]Department of Biology, Washington University in St. Louis, 1 Brookings Drive, St. Louis, MO 63130, USA
*Correspondence: rdvierstra@wustl.edu
http://dx.doi.org/10.1016/j.celrep.2016.07.015

SUMMARY

The autophagic clearance of 26S proteasomes (proteaphagy) is an important homeostatic mechanism within the ubiquitin system that modulates proteolytic capacity and eliminates damaged particles. Here, we define two proteaphagy routes in yeast that respond to either nitrogen starvation or particle inactivation. Whereas the core autophagic machineries required for Atg8 lipidation and vesiculation are essential for both routes, the upstream Atg1 kinase participates only in starvation-induced proteaphagy. Following inactivation, 26S proteasomes become extensively modified with ubiquitin. Although prior studies with *Arabidopsis* implicated RPN10 in tethering ubiquitylated proteasomes to ATG8 lining the autophagic membranes, yeast proteaphagy employs the evolutionarily distinct receptor Cue5, which simultaneously binds ubiquitin and Atg8. Proteaphagy of inactivated proteasomes also requires the oligomeric Hsp42 chaperone, suggesting that ubiquitylated proteasomes are directed by Hsp42 to insoluble protein deposit (IPOD)-type structures before encapsulation. Together, Cue5 and Hsp42 provide a quality control checkpoint in yeast directed at recycling dysfunctional 26S proteasomes.

INTRODUCTION

Constant re-modeling of proteomes is critical for developmental transitions, maintenance of cellular homeostasis in response to environmental challenges, and robust nutrient recycling. In eukaryotes, these adjustments are mainly performed by two proteolytic routes, the ubiquitin-26S proteasome system (UPS) and autophagy. Together, they direct the turnover of a wide array of targets, ranging from single proteins whose control is necessary for proper growth and development, to whole organelles when they become defective or unnecessary. The UPS consists of a highly polymorphic enzymatic cascade that attaches multiple ubiquitins to selected target proteins, which enables their recognition and subsequent degradation by the 26S proteasome (Bhattacharyya et al., 2014; Finley et al., 2016; Lu et al., 2015). In contrast, autophagy is uniquely designed to eliminate larger structures, which are encapsulated and delivered in bulk from the cytoplasm to either vacuoles (plants and fungi) or lysosomes (mammals) for breakdown (Klionsky and Schulman, 2014; Reggiori and Klionsky, 2013).

Autophagy occurs continuously at a basal level, but is upregulated when extensive recycling is required, such as during nutrient starvation or programmed cell death. It is initiated at the phagophore assembly site (PAS), where a collection of factors builds the engulfing phagophore membrane, which then seals to trap cargo within a double membrane-bound autophagosome (Lamb et al., 2013; Reggiori and Klionsky, 2013). Autophagosomes fuse with the limiting membrane of the vacuole to release the internal vesicle as an autophagic body, which is then eliminated by resident hydrolases. Central to this process is the ubiquitin-fold protein Atg8 (or LC3), which becomes modified at its C terminus with phosphatidylethanolamine (PE) via a conjugation cascade analogous to ubiquitylation. The Atg8-PE adduct decorates the expanding phagophore, thus providing docking sites for proteins that promote vesicle closure and for receptors that recruit specific cargo. By virtue of an expansive list of such receptors, autophagy can selectively remove large protein complexes, insoluble aggregates, whole organelles, and even invading intracellular pathogens (Khaminets et al., 2016; Lu et al., 2014; Mochida et al., 2015; Rogov et al., 2014; Sica et al., 2015).

Although the UPS and autophagy were initially thought to operate independently, recent work has revealed considerable overlap between the two systems. In particular, many targets of selective autophagy first require ubiquitylation, which allows their recognition by receptors that simultaneously bind both Atg8 and ubiquitin through an Atg8-interacting motif (AIM) and various ubiquitin-binding domains, respectively. Examples include optineurin and NDP52, which are recruited to both ubiquitylated pathogens and mitochondria (Lazarou et al., 2015; Wild et al., 2011), p62/SQSTM1 and NBR1, which bind to various ubiquitylated cargo including protein aggregates, pathogens, and peroxisomes (Khaminets et al., 2016; Rogov et al., 2014), and Cue5 from the yeast *Saccharomyces cerevisiae* and its mammalian counterpart Tollip, which bind ubiquitylated protein

aggregates (Lu et al., 2014). Through the action of these receptors, ubiquitin addition and autophagy collectively facilitate the breakdown of substrates beyond the architectural constraints of the 26S proteasome.

The 26S proteasome itself is an ATP-dependent, self-compartmentalized proteolytic machine located in the cytosol and nucleus (Bhattacharyya et al., 2014; Finley et al., 2016). It consists of two functionally distinct sub-complexes, namely the 20S core protease (CP) and its 19S regulatory particle (RP). The CP is a barrel generated by four stacked heteroheptameric rings of seven α- and seven β-subunits assembled in a C2 symmetric $\alpha_{1-7}/\beta_{1-7}/\beta_{1-7}/\alpha_{1-7}$ configuration. Six peptidase catalytic sites provided by the β_1, β_2, and β_5 subunits (Pre3, Pup1, and Pre2, respectively, in yeast) are located in the central chamber. Access to this chamber is restricted by gated axial pores formed by the α-rings, through which only unfolded polypeptides can enter. The CP is capped at one or both ends by the 19 subunit RP, which provides activities associated with target recognition, unfolding, and import, plus ubiquitin release prior to target breakdown. Particularly important are receptors for ubiquitylated substrates, including the intrinsic subunits Rpn1, Rpn10, Rpn13, and Sem1 that have affinity for poly-ubiquitin chains, and the extra-proteasomal ubiquitin-binding shuttle factors such as Rad23, Dsk2, and Ddi1 that associate transiently (Farmer et al., 2010; Fatimababy et al., 2010; Finley, 2009; Paraskevopoulos et al., 2014; Shi et al., 2016).

As the final executioner of the UPS, the 26S proteasome is controlled at multiple levels (Schmidt and Finley, 2014). When proteolytic demand is high, especially under proteotoxic stress, genes encoding the full complement of subunits and associated factors are coordinately upregulated through a "proteasome stress" regulon involving one or more dedicated transcriptional regulators (Gladman et al., 2016; Radhakrishnan et al., 2010; Sha and Goldberg, 2014; Xie and Varshavsky, 2001). In yeast, the main regulator is the proteasome substrate Rpn4; its rapid turnover when proteolytic demand is low and slow turnover during proteotoxic stress allows Rpn4 to modulate proteasome capacity transcriptionally (Xie and Varshavsky, 2001). Following synthesis, assembly of the CP and RP particles and final construction of the 26S complex are choreographed by a suite of dedicated chaperones (Tomko and Hochstrasser, 2013). The reversible assembly/disassembly between the 26S complex and the free CP and RP is also regulated, especially upon carbon starvation and mitochondrial stress (Bajorek et al., 2003; Livnat-Levanon et al., 2014). Additionally, carbon starvation in yeast stimulates the deposition of excess nuclear proteasomes, together with the CP chaperone/regulator Blm10, into cytoplasmic proteasome storage granules (PSGs), which are rapidly re-mobilized to the nucleus upon return to carbon-rich media (Laporte et al., 2008). Finally, we recently discovered in *Arabidopsis* that the abundance of 26S proteasomes is regulated by autophagic turnover in a process called proteaphagy (Marshall et al., 2015; Marshall and Vierstra, 2015). This can be separately stimulated by nitrogen starvation, which promotes bulk autophagy, and chemical or genetic inhibition, via a selective route designed to remove dysfunctional 26S proteasomes. This latter route involves extensive ubiquitylation of inactive particles, facilitating their recognition by RPN10, which simultaneously binds the attached ubiquitin moieties through a ubiquitin-interacting motif (UIM), and ATG8 lining the engulfing autophagic membranes through a previously unknown AIM (Marshall et al., 2015).

Although we anticipate that similar proteaphagy routes exist in other eukaryotes, how they work mechanistically, whether ubiquitylation is a prerequisite, and whether RPN10 orthologs participate were unclear, especially given the absence of obvious Atg8-binding sites in the animal and yeast Rpn10 sequences (Marshall et al., 2015). In an attempt to confirm proteaphagy outside of plants and define the receptor(s) involved, we studied 26S proteasome turnover in yeast. Along with a companion paper by Waite et al. (2016), we here describe yeast proteaphagy, including the discovery of separate routes employed during nitrogen starvation and proteasome inactivation. We also show that inactivated proteasomes become extensively ubiquitylated, and surprisingly find that the extra-proteasomal ubiquitin receptor Cue5, which is evolutionarily unrelated to RPN10, is required for the autophagic clearance of damaged particles. Also essential is the Hsp42 chaperone, which was previously shown to promote protein quality control through the assembly of insoluble protein deposit (IPOD) structures (Kaganovich et al., 2008; Malinovska et al., 2012; Peters et al., 2015; Specht et al., 2011). Together, Cue5 and Hsp42 provide an important proteasome surveillance mechanism in yeast (and likely animals) that is central to maintaining a healthy pool of active 26S particles.

RESULTS

The 26S Proteasome Is Subject to Proteaphagy in Yeast

As a first step to investigate proteasome turnover in yeast, we developed growth conditions to examine autophagy induced by either nitrogen starvation or proteasome inactivation via the CP active site inhibitor MG132. Nitrogen starvation rapidly suppressed culture growth and led to a steady decline in total cell protein (Figures S1A and S1B). It also induced bulk autophagy, as demonstrated by the accumulation of free GFP proteolytically released from the GFP-Atg8 reporter (Figure S1C), which has been previously shown to occur in the vacuole by an autophagy-dependent process (Klionsky et al., 2016), and by the increased activity of the engineered Pho8Δ60 reporter (Figure S1D), which requires autophagic transport to the vacuole for proteolytic activation (Noda and Klionsky, 2008).

Although wild-type yeast is generally impermeable to MG132, several conditions have been reported that improve uptake, and thus efficacy, namely the use of an SDS-containing medium in which the main nitrogen source is proline (Liu et al., 2007), or using the Δ*erg6* background that increases membrane permeability by eliminating ergosterol biosynthesis (Lee and Goldberg, 1996). Unfortunately, the proline/SDS medium slightly activated bulk autophagy by itself (presumably because of restricted nitrogen availability), as judged by modest accumulation of free GFP from GFP-Atg8 and activation of the Pho8Δ60 reporter (Figures S1C and S1D). In contrast, MG132 in the Δ*erg6* background did not activate bulk autophagy but effectively inhibited proteasomes, based on a suppression of culture growth and activation of the proteasome-stress regulon induced by Rpn4 (Figures

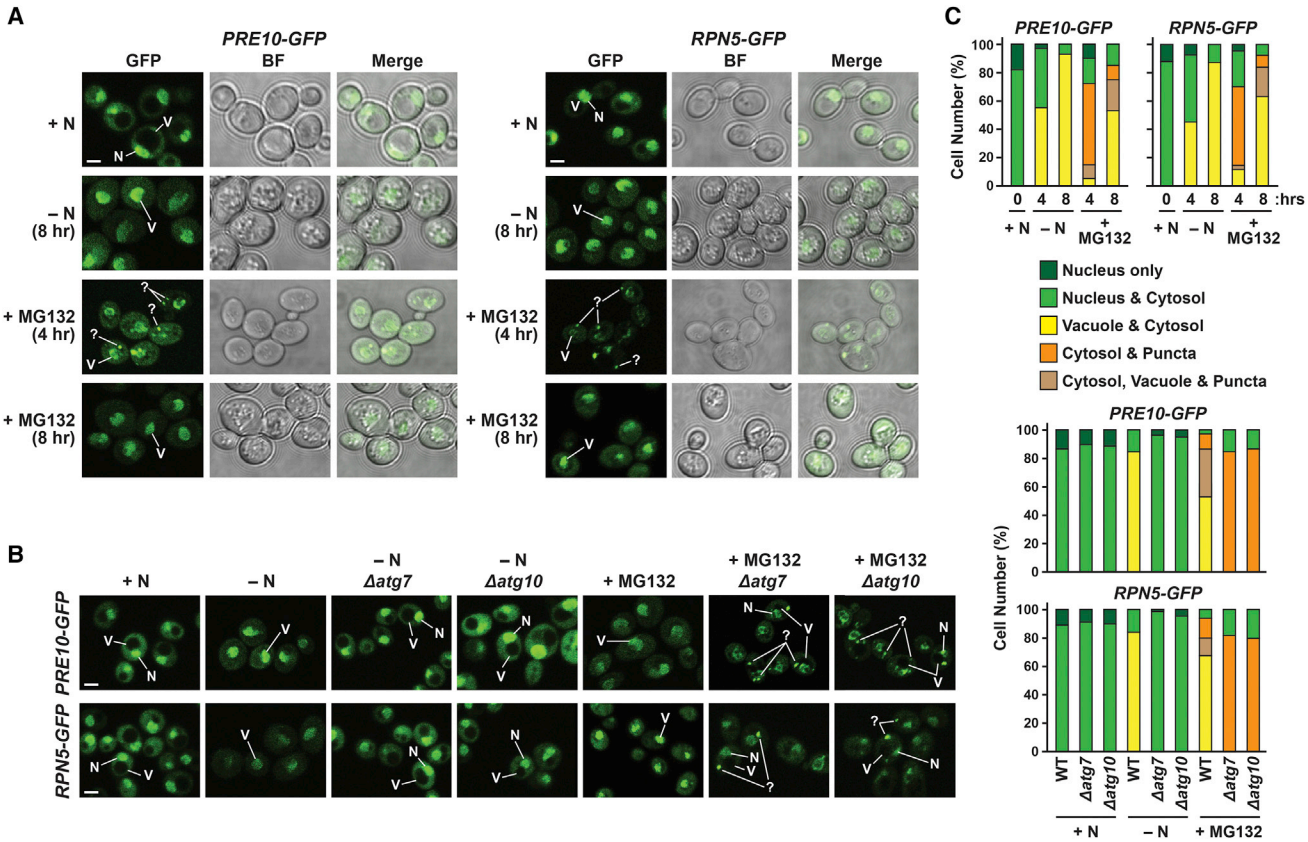

Figure 1. Yeast 26S Proteasomes Are Delivered to the Vacuole by Autophagy

(A) 26S proteasomes are transported to the vacuole during nitrogen (N) starvation or upon inactivation by the proteasome inhibitor MG132. Cells expressing *PRE10-GFP* (left panels) or *RPN5-GFP* (right panels) were grown on +N medium and either switched to –N or +MG132 (80 μM) media for the indicated times. Cells were then imaged by confocal fluorescence microscopy. Shown are the fluorescence (GFP), bright field (BF), and merged images. N, nucleus; V, vacuole; ? identifies cytoplasmic puncta similar to IPOD structures (also applies in B). Scale bar, 2 μm.

(B) The localization of 26S proteasomes to the vacuole is directed by Atg8-mediated autophagy. Shown are representative wild-type, Δ*atg7*, or Δ*atg10* cells expressing *PRE10-GFP* or *RPN5-GFP* imaged 8 hr after transfer to –N or +MG132 (80 μM) media. Scale bar, 2 μm.

(C) Quantification of the cellular distribution of 26S proteasomes as visualized in (A) and (B). Cells were grown with or without N starvation or 80 μM MG132 for the indicated periods of time. Each bar represents analysis of at least 200 cells. For the MG132 assays in (A), (B) and (C), the cells also harbored the Δ*erg6* mutation. See also Figure S1.

S1A–S1C and S2). Consequently, the Δ*erg6* background was exploited in all subsequent assays using the inhibitor.

Our previous methods to track proteaphagy in *Arabidopsis* relied on tagged proteasomes in which individual subunits were substituted in planta with GFP fusions, which we then exploited to follow autophagic transport to the vacuole by fluorescence microscopy, and to monitor vacuolar breakdown by the release of free GFP from the fusion (Marshall et al., 2015). Here, we developed similar assays using available yeast strains in which the essential CP subunit Pre10 (α_7) and the RP subunit Rpn5 were genetically replaced with versions bearing a C-terminal GFP. Rescue of the lethal phenotype of Δ*pre10* and Δ*rpn5* cells by these GFP fusions confirmed their functionality (Figure 1A) (Fujiwara et al., 1990; Saito et al., 1997).

During exponential growth in nitrogen-rich YPDA medium, much of the cellular fluorescence from Pre10-GFP and Rpn5-GFP was observed in the nucleus (Figures 1A–1C), in agreement with the nuclear-enriched distribution of yeast 26S proteasomes. However, upon nitrogen starvation, the nuclear signal steadily diminished and a strong diffuse fluorescence concomitantly appeared in the vacuole (Figures 1A and 1B), which was consistent with the GFP fusions entering the vacuole via autophagosomes, followed by breakdown of the autophagic bodies and release of the GFP moiety into the vacuole lumen. A strikingly different response was seen in *PRE10-GFP* Δ*erg6* and *RPN5-GFP* Δ*erg6* cells exposed to 80 μM MG132. Instead of appearing to move directly from the nucleus to the vacuole, bright cytoplasmic puncta became evident at early time points (4 hr), which was followed by the accumulation of diffuse vacuolar fluorescence at 8 hr (Figures 1A and 1B), suggesting that cytoplasmic aggregation of inactivated 26S proteasomes precedes their autophagic clearance.

That this vacuolar accumulation during either nitrogen starvation or MG132-induced inactivation was driven by an Atg8-mediated pathway was confirmed by localization of the Pre10-GFP and Rpn5-GFP fluorescence in the Δ*atg7* and

Δ*atg10* backgrounds, which cannot assemble the Atg8-PE adduct needed to direct autophagy (Reggiori and Klionsky, 2013). In both strains, movement of the nuclear GFP signal to the vacuole was not apparent in nitrogen-starved cells (Figures 1B and 1C). Such movement was similarly blocked by the Δ*atg7* and Δ*atg10* mutations upon MG132 treatment but, surprisingly, GFP fluorescence still accumulated in cytoplasmic puncta (Figures 1B and 1C), suggesting that formation of these foci is upstream of autophagic vesiculation.

To more easily follow proteaphagy, we monitored the release of free GFP from the Pre10-GFP and Rpn5-GFP fusions by immunoblotting total cell lysates with anti-GFP antibodies. Densitometric scans of the blots then allowed us to quantify the process as a percentage of total GFP released as free GFP, with the value for total GFP at 0 hr assigned as 100%. As shown in Figures 2A and 2B, this cleavage was minimal under nitrogen-rich growth conditions, but was strongly stimulated by nitrogen starvation. In fact, the GFP fusions were largely absent after 20 hr, with more than 80% of the GFP now in a free form, indicating that much of the 26S proteasome pool is eliminated by proteaphagy during nitrogen stress.

In line with the poor permeability of MG132, its stimulation of proteaphagy was minimal in wild-type yeast, but was strongly increased when combined with the Δ*erg6* deletion. However, levels of the GFP fusions did not decline in Δ*erg6* cells, and in fact, the percentage of total GFP released rose well above 100% (Figure 2B), suggesting that transcriptional upregulation of the proteasome-stress regulon by Rpn4 augmented proteasome synthesis under such stress. This upregulation was confirmed by qRT-PCR analysis of representative CP and RP genes; whereas mRNA levels rose substantially upon exposure of Δ*erg6* cells to MG132, this rise was absent in Δ*erg6* Δ*rpn4* cells (Figures 2C and S2). When subsequently applied to the free GFP assays, we could now detect a substantial loss of the Pre10-GFP and Rpn5-GFP fusions in the Δ*erg6* Δ*rpn4* backgrounds during MG132 treatment, with the percentage of total GFP released now asymptotically approaching 100% of the initial GFP fusion pool (Figures 2A and 2B). Notably, the loss of 26S proteasome subunits during nitrogen starvation or MG132 treatment was not restricted to the Pre10-GFP and Rpn5-GFP reporters. A steady disappearance of Pre4 (β_7) from the CP and Rpt1, untagged Rpn5, and Rpn8 from the RP, was observed when wild-type cells were starved for nitrogen or when Δ*erg6* Δ*rpn4* cells were exposed to 80 μM MG132 (Figure 2D).

It was conceivable that MG132-induced proteaphagy is part of a larger bulk autophagic process that also degrades non-proteasomal substrates or impacts protein transport through the cytoplasm-to-vacuole targeting (CVT) pathway (Reggiori and Klionsky, 2013). To discount this possibility, we tested the effects of MG132 on the turnover of GFP-tagged substrates known to be removed by mitophagy (Om45-GFP), pexophagy (Pex14-GFP), or ribophagy (Rpl25-GFP), or localized to the vacuole via the CVT (GFP-Ape1) (Khaminets et al., 2016). In each case, release of free GFP from the fusions was readily evident upon nitrogen starvation of wild-type cells, but was absent in MG132-treated Δ*erg6* cells (Figure S3), strongly suggesting that MG132 treatment specifically induces proteaphagy.

Consistent with the fluorescence microscopy studies, proteaphagy of GFP-labeled proteasomes, as measured by the appearance of free GFP, was blocked in the Δ*atg7* and Δ*atg10* backgrounds, demonstrating that Atg8-mediated autophagy was involved (Figure 3A). We also confirmed that release of free GFP occurred in the vacuole by exploiting cells missing Pep4, the vacuolar processing protease that is required for the activation of many vacuolar hydrolases (Woolford et al., 1986). As shown in Figure 3B, the release of free GFP from either reporter was effectively eliminated in nitrogen-starved or MG132-treated Δ*pep4* cells.

To further define which activities central to the core autophagy system also participate in proteaphagy, we tested mutants missing subunits of the upstream Atg1 kinase complex (Atg1, Atg11, Atg13, and Atg17) that integrates various stress signals including those from central nutrient sensors such as Tor1/2, the Atg9 complex (Atg2, Atg9, and Atg18) that delivers membranes to the expanding phagophore, and the phosphatidylinositol 3-kinase (PI3K) complex (Atg6/Vps30, Atg14, Vps15, and Vps34) that decorates the phagophore membrane with PI3P (Reggiori and Klionsky, 2013). Based on the free GFP release assay, mutants defective in the Atg9 complex blocked both nitrogen-starvation and MG132-induced proteaphagy, while mutants in the PI3K complex showed a consistent dampening of both routes, indicating that the former activity is essential to proteaphagy, whereas the latter is important but not required (Figures S4B and S4C). In contrast, we found that the Atg1 kinase is essential for proteaphagy induced by nitrogen starvation, but is not needed for proteaphagy induced by MG132 (Figures 3A and S4A). This demarcation is similar to our observations with *Arabidopsis* (Marshall et al., 2015) and indicates that two proteaphagic routes also exist in yeast, one dependent on nutritional signals impinging on the Atg1 kinase and another immune to its action. We note that the collection of mutants impacting each of the three Atg complexes affected proteaphagy similarly (strong/partial inhibition or no effect), consistent with the expectation that each subunit is crucial to the activities of their respective complexes (Reggiori and Klionsky, 2013).

Cue5 Is the Receptor for Proteaphagy of Inactivated Proteasomes

Next, we attempted to identify the receptor(s) that direct proteaphagy. Whereas the *Arabidopsis* proteaphagy receptor for nitrogen starvation is not yet known, the receptor for inactivated proteasomes was shown to be the ubiquitin-binding protein RPN10, which exists in both a free form and as part of the RP (Marshall et al., 2015). However, initial tests with the Δ*rpn10* strain revealed that its yeast counterpart is not involved in either nitrogen starvation- or MG132-induced proteaphagy (Figure 3A). In support of this finding, yeast Rpn10 does not have an obvious AIM and did not recognize Atg8 by yeast two-hybrid (Y2H) assays (Figure S5A).

Subsequently we tested whether alternative ubiquitin receptors that associate with the proteasome, including the core subunits Rpn13 and Sem1 and the shuttle factors Rad23, Dsk2, and Ddi1 (Finley, 2009; Fatimababy et al., 2010; Paraskevopoulos et al., 2014), substitute for Rpn10 in yeast proteaphagy.

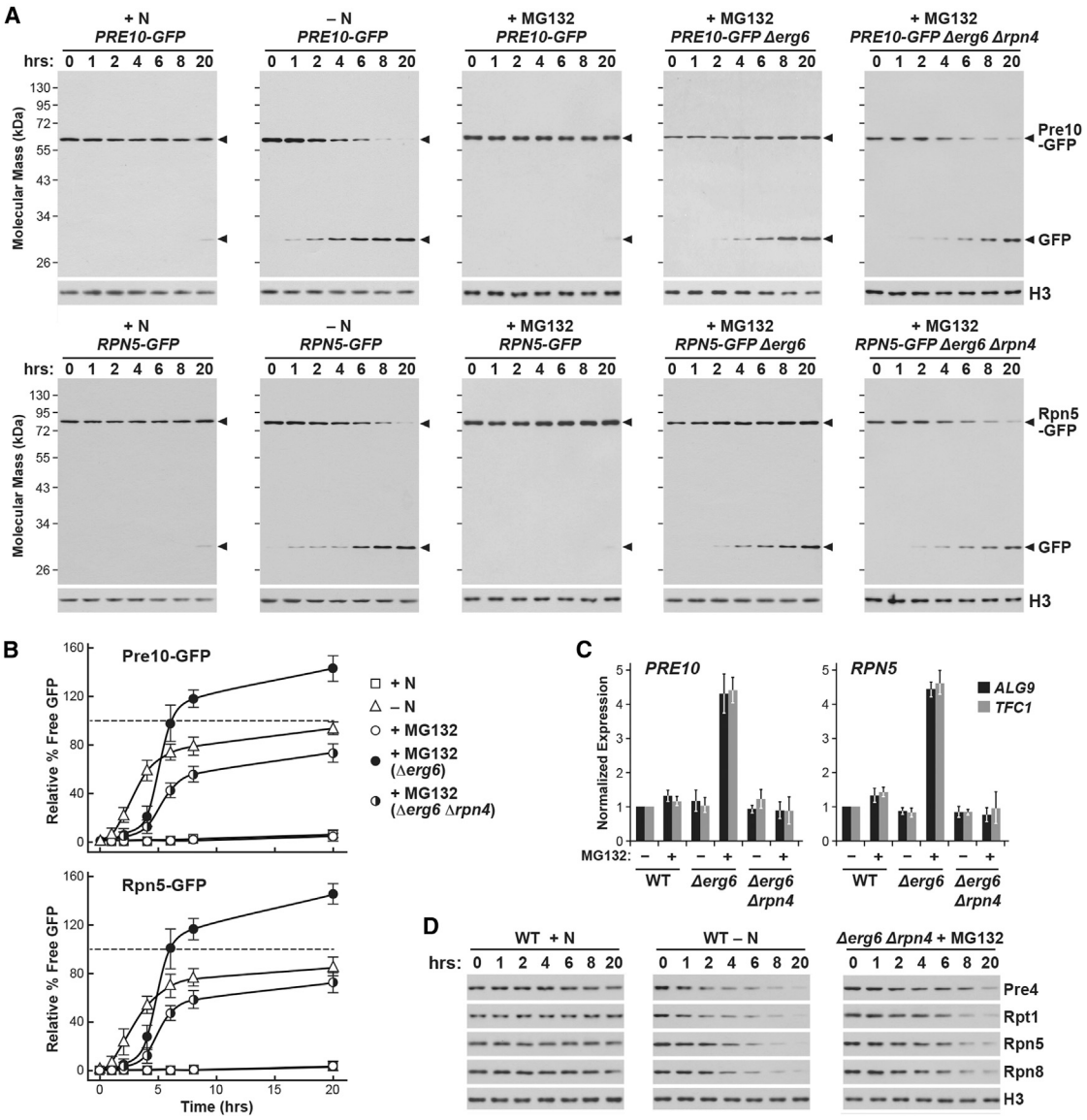

Figure 2. Demonstration of Yeast Proteaphagy Based on the Proteolytic Release of Free GFP from the Pre10-GFP and Rpn5-GFP Reporters

Cells expressing Pre10-GFP or Rpn5-GFP with or without the Δ*erg6* and/or Δ*rpn4* mutations were grown on +N medium and then switched to either –N or +MG132 (80 μM) media for the indicated periods of time.

(A) Time course of free GFP release from Pre10-GFP or Rpn5-GFP. Cells were harvested at the indicated times and assayed for the accumulation of free GFP by immunoblot analysis with anti-GFP antibodies. Arrowheads locate the GFP fusion and free GFP. Immunodetection of histone H3 was included to confirm near equal protein loading.

(B) Quantification of the amount of free GFP released from the Pre10-GFP (top) or Rpn5-GFP (bottom) fusions by densitometric scans of the blots shown in (A). For both reporters, the amount of GFP fusion protein present at 0 hr was set as 100%. Bars represent the mean (±SD) of three biological replicates.

(C) Effect of MG132 on the expression of the endogenous *PRE10* and *RPN5* genes. Total RNA was isolated from WT, Δ*erg6*, and Δ*erg6* Δ*rpn4* cells after an 8 hr incubation with or without 80 μM MG132. Relative transcript abundance was determined by quantitative real-time PCR, using the *ALG9* or *TFC1* transcripts as internal reference standards. All data points were normalized to untreated WT cells. Bars represent the mean (±SD) of three biological replicates. Analysis of additional proteasome subunit genes is shown in Figure S2.

(D) Effect of N starvation or MG132 inhibition on the steady state levels of 26S proteasome subunits. WT or Δ*erg6* Δ*rpn4* cells were grown in +N medium and then switched to either –N or +MG132 (80 μM) media for the indicated periods of time. Total protein extracts were then probed with antibodies against the indicated proteasome subunits, with immunodetection of histone H3 included to confirm near equal protein loading.

See also Figures S2 and S3.

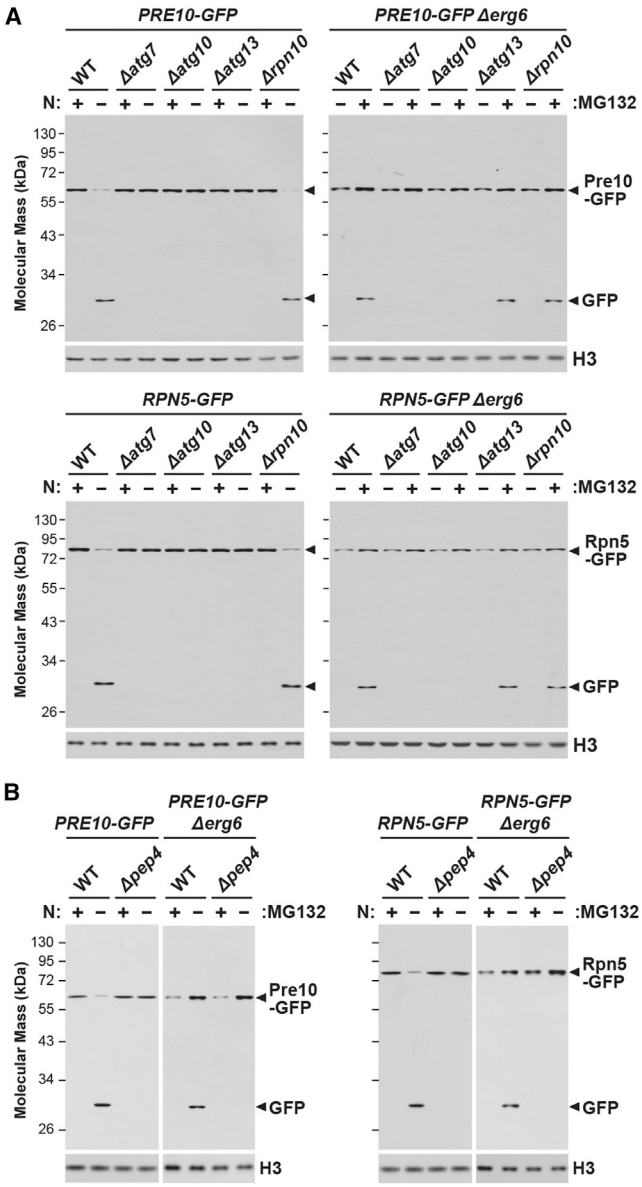

Figure 3. Proteaphagy in Yeast Requires the Atg8-Mediated Autophagic System

(A) Autophagy pathway mutants (Δ*atg7*, Δ*atg10*, and Δ*atg13*), but not a mutant missing the ubiquitin receptor Rpn10, block proteaphagy. The indicated mutations were combined with the *PRE10-GFP* or *RPN5-GFP* backgrounds, with or without the Δ*erg6* mutation. Cells were grown on +N medium and then switched to either –N or +MG132 (80 μM) media for 8 hr. Release of free-GFP from the reporters was assayed by immunoblot analysis of total cell extracts with anti-GFP antibodies, as in Figure 2. Immunodetection of histone H3 was included to confirm near equal protein loading.

(B) The release of free GFP from Pre10-GFP and Rpn5-GFP occurs in the vacuole. Cells expressing *PRE10-GFP* or *RPN5-GFP*, with or without the Δ*erg6* mutation, were combined with the Δ*pep4* mutation that blocks vacuolar protease maturation. Cells were then assayed for the release of free GFP after 8 hr growth on –N or +MG132 media, as in (A).

See also Figure S4.

However, based on the GFP cleavage assay, none of the corresponding deletion mutants impacted either nitrogen starvation- or inhibitor-induced proteaphagy (Figure S4D). To expand the search, we then tested most of the known selective autophagy receptors in yeast for their effects on either proteaphagic route, including Atg19 (CVT), Atg32 (mitophagy), Atg34 (CVT), Atg36 (pexophagy), Atg39 (nucleophagy), Atg40 (reticulophagy), and Cue5 (aggrephagy) (Khaminets et al., 2016). As shown in Figure 4A, most of the corresponding deletions strains introduced into cells expressing the Pre10-GFP or Rpn5-GFP reporters failed to block the autophagic release of free GFP during either nitrogen starvation or MG132 exposure.

Strikingly, the lone exception was Cue5, deletion of which effectively stopped the MG132-induced proteaphagic route, but not that for nitrogen starvation. Cue5 is part of an eight-member protein family defined by a signature 43-amino-acid CUE domain that binds ubiquitin (Figures S6A and S6B) (Kang et al., 2003; Shih et al., 2003). However, Cue5 is distinct by also containing a WQPL AIM sequence (residues 373–376) that binds Atg8 (Lu et al., 2014). We confirmed the specificity of this binding by Y2H assays; only Cue5 among several other members of the Cue family, including its closest phylogenetic relative Don1, displayed a strong Y2H interaction with Atg8 (Figures 4B and S6C). The specificity of Cue5 for MG132-induced proteaphagy was then demonstrated by comparing Pre10-GFP or Rpn5-GFP cleavage in deletion backgrounds impacting each of the eight Cue domain-containing proteins. Only the Δ*cue5* strains failed to accumulate free GFP from either reporter upon MG132 treatment (Figure 4C).

The importance of Cue5 to proteaphagy of inactivated 26S particles was also demonstrated by confocal fluorescence microscopy of the Pre10-GFP and Rpn5-GFP reporters expressed in the Δ*cue5* background. Whereas the *Δcue5* cells still accumulated GFP fluorescence in the vacuole upon nitrogen starvation, this accumulation was absent following MG132 exposure, as compared to a *CUE5-HA*-complemented Δ*cue5* strain (Figures 4D and 4E). Instead, cytoplasmic puncta persisted in MG132-treated Δ*cue5* cells, suggesting that Cue5 is not required for the aggregation of inactivated 26S proteasomes, but is needed for their vacuolar deposition.

Genetically Compromised 26S Proteasomes Also Undergo Proteaphagy

For additional confirmation that the response to MG132 reflected the clearance of dysfunctional proteasomes through an autophagic process requiring Cue5, we examined the release of free GFP from proteasomes compromised genetically. Here, we exploited the *doa5-1* and *rpn5ΔC* mutations affecting the Pup2 (α_5 of the CP) and Rpn5 subunits, respectively. The *doa5-1* allele contains a single amino acid substitution in Pup2 that generates temperature-sensitive lethality and displays other pleiotropic phenotypes, including reduced sporulation and sensitivity to canavanine and high salt (Chen and Hochstrasser, 1995), whereas the *rpn5ΔC* allele expresses a truncation missing the last 34 residues of Rpn5, which also elicits temperature-sensitivity and compromises proteasome lid assembly (Peters et al., 2015).

When the *doa5-1* mutation was introduced into the *PRE10-GFP* strain, we detected release of free GFP, indicating that

damage of one CP subunit can stimulate the degradation of another functional CP subunit, presumably by proteaphagy of the entire complex (Figure 5A). This release was abrogated in either the Δ*atg7 doa5-1* or Δ*cue5 doa5-1* backgrounds, as expected if autophagy and Cue5 were involved. Similar effects were observed in cells expressing additional GFP-tagged CP subunits (Pre6 [α_4] and Pup1 [β_2]), with free GFP being released when the *doa5-1* mutation was present and this release being blocked in Δ*atg7* and Δ*cue5* backgrounds (Figure 5A). Likewise, we found that free GFP could be released either from the GFP-Rpn5ΔC truncation when used to complement the *rpn5ΔC* mutation (Figure 5B) or from the Rpt6-GFP and Rpn12-GFP fusions when expressed in the *rpn5ΔC* background (Figure 5C). These releases were also abrogated in the Δ*atg7* or Δ*cue5* backgrounds, indicating that the *rpn5ΔC* mutation stimulates proteaphagy of the entire RP (and not just Rpn5ΔC) via a Cue5-dependent mechanism (Figures 5B and 5C).

Surprisingly, we found that release of GFP from Pre6-GFP, Pre10-GFP, or Pup1-GFP was not evident in *rpn5ΔC* cells, suggesting that damage to the RP does not a priori stimulate proteaphagy of the CP (Figure 5A). In a similar fashion, release of free GFP from Rpt6-GFP, GFP-Rpn5, or Rpn12-GFP was not evident in the *doa5-1* cells, suggesting that damage to the CP does not a priori stimulate proteaphagy of the RP (Figures 5B and 5C). Collectively, it appears that proteaphagy can eliminate the entire 26S particle, as is the case with MG132 inactivation, or in some situations can remove damaged CP or RP selectively.

MG132 Triggers Ubiquitylation of Proteasomes and Association of Cue5

The involvement of Cue5 led us to predict that proteaphagy of damaged 26S proteasomes is triggered by ubiquitylation, as we first observed with *Arabidopsis* (Marshall et al., 2015). To support this mechanism, we analyzed 26S proteasomes isolated from wild-type cells grown in nitrogen-rich or poor media, or from Δ*erg6* cells treated with 80 μM MG132, by using purification strains in which the Pre1 (β_4), Rpt1, or Rpn11 subunits had been genetically replaced with Protein A (ProA)-TEV-tagged versions (Leggett et al., 2005). The resulting preparations obtained by IgG affinity chromatography in the presence of ATP contained the characteristic SDS-PAGE ladder of 26S subunits irrespective of growth conditions and included near equal levels of representative CP and RP subunits (Figures 6A and 6B), showing that nitrogen starvation and MG132 exposure does not dramatically change particle composition. The only notable differences were slightly increased association of the CP and RP upon MG132 treatment, consistent with prior observations that proteasome inhibition strengthens this interaction (Kleijnen et al., 2007) and an increased binding of the alternative capping particle Blm10, as was also observed for its *Arabidopsis* counterpart PA200 (Marshall et al., 2015). However, when assayed for ubiquitin by immunoblotting, a strong increase in ubiquitylation was evident in the MG132-treated preparations (Figure 6A). Whereas only a few subunits in the high apparent molecular mass region (likely Rpn1 and Rpn2) (Book et al., 2010) were ubiquitylated in nitrogen-rich and nitrogen-starved cells, a diverse array of adducts became prevalent in MG132-treated particles (Figure 6A).

To better define the composition of these 26S proteasome preparations, we subjected them to trypsinization followed by tandem mass spectrometry (MS). As expected based on SDS-PAGE profiles, all the core CP and RP subunits were detected at near equal levels in nitrogen-rich, nitrogen-starved, and MG132-treated samples enriched via the Pre1, Rpt1, or Rpn11 subunits (see Figure 6C for representative subunits). Strikingly, we also selectively detected high levels of Cue5 in the MG132-treated samples. Label-free MS quantification based on peptide peak areas revealed a >1,000-fold increase in Cue5 (Figure 6C), demonstrating that proteasome inactivation strongly encouraged Cue5 association, presumably through the attached ubiquitin moieties.

To confirm this scenario, we purified proteasomes from MG132-treated cells via the Pre1 and Rpn11 subunits and trimmed the attached ubiquitin moieties with the deubiquitylating enzyme USP2 (Besche et al., 2014). While the subunit composition of the proteasomes was unaffected by USP2 incubation (Figures S7A and S7B), immunoblot analyses showed that the level of associated ubiquitin was reduced by ~65%–70% (Figure S7A). Label-free MS quantification then showed that, while a >1,000-fold increase in Cue5 association was again observed upon MG132 treatment, its occupancy was reduced by over 80% upon USP2 treatment, indicating that Cue5 binds to ubiquitin moieties associated with the proteasome (Figure S7C). To further connect proteasome ubiquitylation to autophagic turnover, we examined proteasomes affinity-enriched from Δ*atg7* or Δ*cue5* backgrounds. Whereas the composition of the 26S proteasome appeared unchanged, an approximately 1.75-fold increase in proteasome ubiquitylation was seen in the mutants as compared to wild-type upon MG132 treatment (Figure S7D).

While proteasome subunits are known to be ubiquitylated upon inhibition of the complex (Kim et al., 2011, 2013), it remained possible that the ubiquitin signal and Cue5 binding observed here upon MG132 treatment was instead caused by increased occupancy of ubiquitylated substrates whose degradation had become stalled by the inhibitor. To help rule out this possibility, we employed two complementary approaches. One was to use a high salt wash during the affinity purification, which has been shown to dissociate loosely-bound substrates awaiting turnover. Whereas this wash step effectively removed the accessory factor Ecm29 (Figure S7E) (Leggett et al., 2002) and likely released ubiquitylated substrates (Peth et al., 2010), no change in the amount of associated ubiquitin was observed (Figure S7E). As a second approach, we compared 26S proteasomes that were purified from untreated cells in the presence of MG132 (i.e., post-lysis inhibition), which presumably would contain ubiquitylated substrates trapped at the point of extraction, to those purified from MG132-treated cells but without MG132 during purification (i.e., pre-lysis inhibition). Such post-lysis treatment was clearly effective at inhibiting the peptidase activity of the proteasome and had little impact on proteasome composition (Figures S7F and S7G). Importantly, while MG132 treatment pre-lysis led to a strongly increased ubiquitin signal associated with the proteasome, the post-lysis treatment did not (Figure S7F). Together, these data indicate that Cue5 likely binds directly to ubiquitylated proteasome subunits, rather than to associated targets awaiting breakdown.

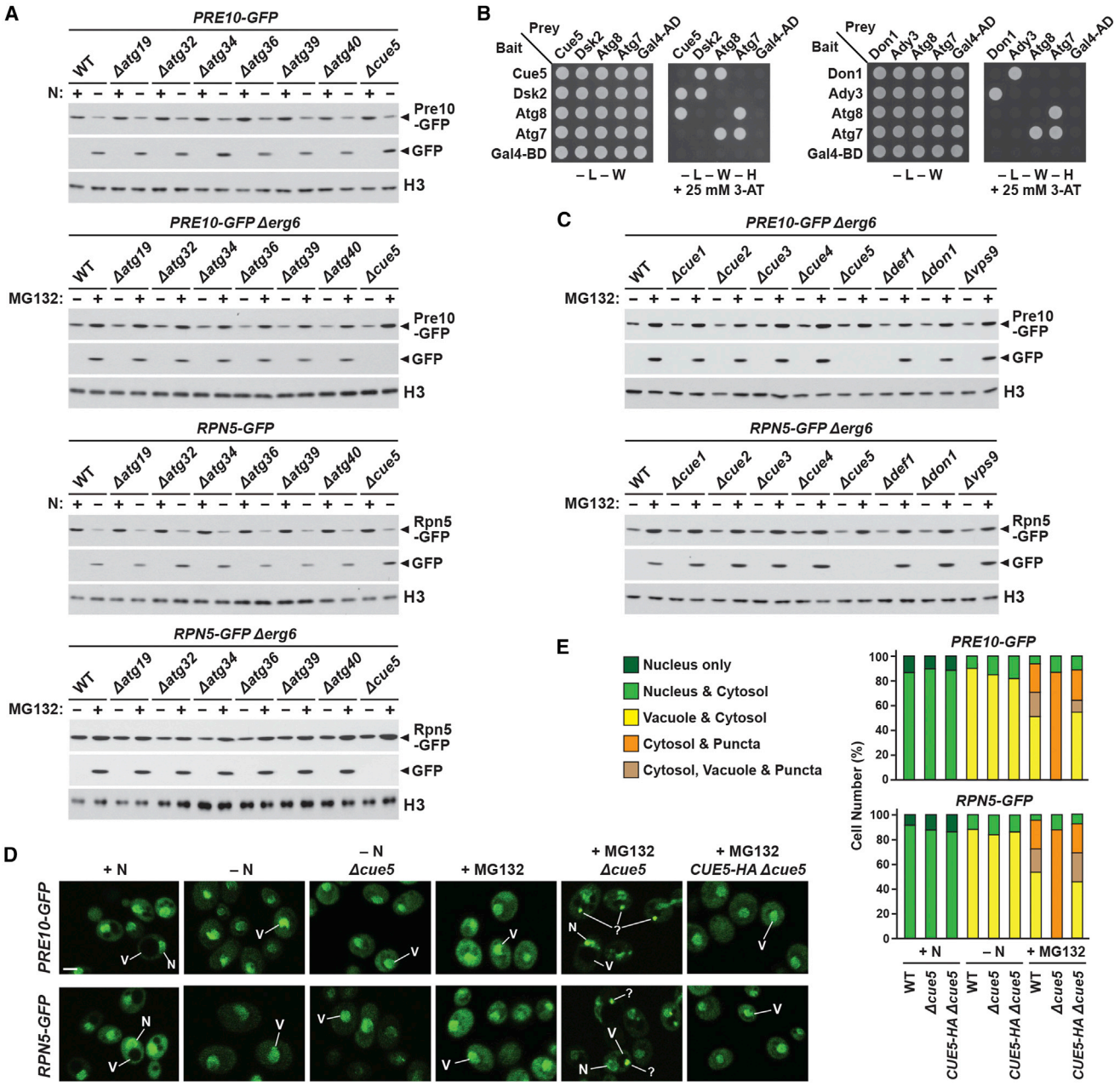

Figure 4. Cue5 Serves as the Proteaphagy Receptor for Inactivated 26S Proteasomes

(A) Mutations affecting possible proteaphagy receptors were combined with the *PRE10-GFP* or *RPN5-GFP* backgrounds, with or without the Δ*erg6* mutation. Cells were grown on +N medium and then switched to either –N or +MG132 (80 μM) media for 8 hr. Autophagy-mediated release of free GFP from the Pre10-GFP and Rpn5-GFP reporters was assayed by immunoblot analysis of total cell extracts with anti-GFP antibodies, as in Figure 2. Only portions of the gel containing the GFP fusions or free GFP are shown. Immunodetection of histone H3 was included to confirm near equal protein loading. Among the various selective autophagy receptors tested, only Cue5 is required for MG132-induced, but not starvation-induced, proteaphagy.

(B) Yeast two-hybrid (Y2H) assays testing the interaction of Cue5 and its closest yeast relative Don1 with Atg8. Full-length proteins fused with either the GAL4 activating (AD) or binding (BD) domains at their N terminus were co-expressed in all pair-wise orientations. Known interactions between Cue5 and Dsk2, Don1 and Ady3, and Atg8 and Atg7 were used as positive controls. Shown are colonies grown on media lacking Leu and Trp, or lacking Leu, Trp and His and containing 25 mM 3-amino-1,2,4-triazole (3-AT). See Figure S6C for the Y2H assays of other Cue family members.

(C) Mutations affecting each of the eight yeast CUE domain-containing proteins were combined with the *PRE10-GFP* or *RPN5-GFP* backgrounds containing the Δ*erg6* mutation. Cells were then grown, treated, and analyzed by immunoblot of total cell extracts with anti-GFP antibodies as in (A). Within the yeast CUE family, only Cue5 mediates MG132-induced proteaphagy.

(legend continued on next page)

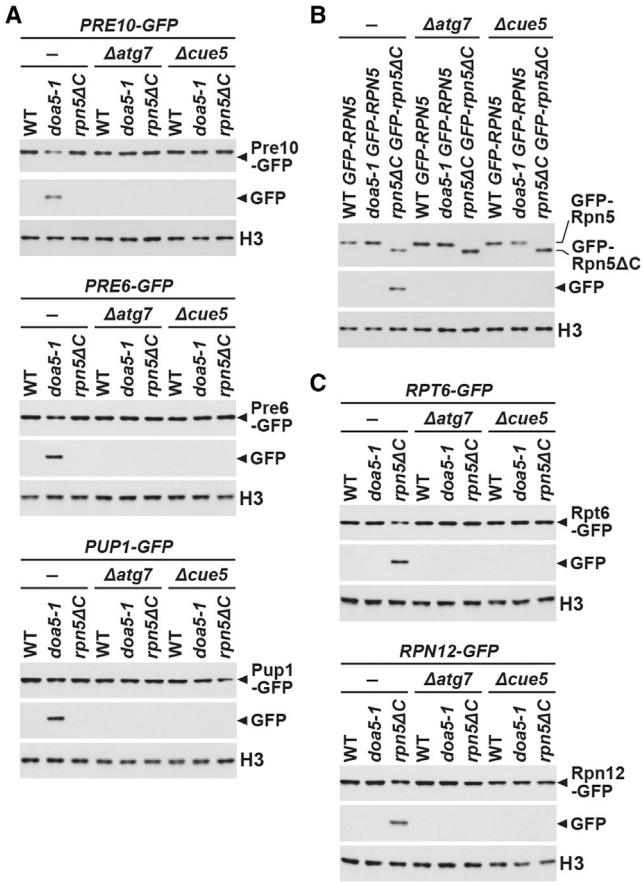

Figure 5. Cue5-Mediated Proteaphagy Is Also Induced by Mutations that Compromise 26S Proteasome Activity or Assembly

(A) Wild-type (–), Δ*atg7*, or Δ*cue5* cells expressing *PRE6-GFP*, *PRE10-GFP*, or *PUP1-GFP* without (WT) or with the *doa5-1* or *rpn5ΔC* mutations that attenuate the activity of the Pup2 (CP) and Rpn5 (RP) subunits of the 26S proteasome were grown on +N medium. Cells were assayed for the release of free GFP from the reporters by immunoblot analysis of total cell extracts with anti-GFP antibodies, as in Figure 2.

(B) Wild-type (–), Δ*atg7*, or Δ*cue5* cells expressing *GFP-RPN5* or *GFP-rpn5ΔC* without (WT) or with the *doa5-1* or *rpn5ΔC* mutations were grown and analyzed as in (A).

(C) Wild-type (–), Δ*atg7*, or Δ*cue5* cells expressing *RPT6-GFP* or *RPN12-GFP* without (WT) or with the *doa5-1* or *rpn5ΔC* mutations were also grown and analyzed as in (A). In (A)–(C), only portions of the gel containing the GFP fusions or free GFP are shown. Immunodetection of histone H3 was included to confirm near equal protein loading.

Cue5 Tethers Ubiquitylated 26S Proteasomes to Atg8

Under the assumption that Cue5 recruits ubiquitylated 26S proteasomes to the autophagic membranes of MG132-treated cells, we tested by co-immunoprecipitation whether Cue5 could simultaneously bind 26S particles and Atg8. Here, we expressed HA-tagged wild-type Cue5, or versions harboring either a mutated CUE domain that blocks ubiquitin binding, or a mutated AIM sequence that blocks interaction with Atg8 (Lu et al., 2014), in Δ*cue5* Δ*erg6* cells. As shown in Figure 6D, immunoprecipitation of wild-type Cue5-HA, but not the Cue5(ΔCUE)-HA or Cue5(ΔAIM)-HA mutants, with anti-HA antibodies co-immunoprecipitated Atg8 together with a diverse profile of ubiquitylated proteins from untreated cells. However, only when the cells were treated with MG132 could wild-type Cue5-HA, but not the mutated versions, simultaneously enrich for Atg8 and representative subunits of the 26S proteasome (Pre4 [β_7] of the CP, and Rpt1, Rpn5, and Rpn8 of the RP), demonstrating that Cue5 can act as a bridge between Atg8 and ubiquitylated proteasomes.

To further confirm that Cue5 needs both its CUE and AIM sequences to direct autophagic clearance of inactivated proteasomes, we combined the Pre10-GFP and Rpn5-GFP reporters with Δ*cue5* strains complemented with HA-tagged versions of either wild-type Cue5 or the Cue5 mutants Cue5(ΔCUE)-HA or Cue5(ΔAIM)-HA. Whereas the release of free GFP from either reporter upon MG132 treatment was not evident in Δ*cue5* cells alone or in Δ*cue5* cells complemented with the mutated Cue5 proteins, it was easily observed in Δ*cue5* cells complemented with wild-type Cue5-HA (Figure 6E).

The Hsp42 Chaperone Controls Proteaphagy of Inactivated 26S Proteasomes

Our detection of cytoplasmic aggregates during the proteaphagy of inactivated 26S proteasomes was reminiscent of prior studies that connected IPOD-type cytoplasmic aggregates to the removal of aberrant proteins (Kaganovich et al., 2008; Malinovska et al., 2012), including mis-assembled subunits of the 26S proteasome (Peters et al., 2015). A key factor in IPOD assembly and subsequent breakdown is Hsp42, an oligomeric chaperone that works with Hsp26 and Hsp104 in sorting misfolded proteins into larger cytoplasmic aggregates (Haslbeck et al., 2004; Miller et al., 2015; Specht et al., 2011). To test for a possible role of these chaperones in proteaphagy, we introduced the Pre10-GFP and Rpn5-GFP reporters into the Δ*hsp26*, Δ*hsp42*, and Δ*hsp104* backgrounds and tested for the release of free GFP upon MG132 treatment. Whereas autophagic clearance of inactivated 26S proteasomes appeared normal in the Δ*hsp26* and Δ*hsp104* strains, it was abolished in the Δ*hsp42* strain, indicating a specific role for this chaperone (Figure 7A).

The Hsp42 polypeptide consists of a 243-residue N-terminal domain (NTD) that is required for substrate recruitment to the IPOD, followed by a 104-residue α-crystallin domain and a 29-residue C-terminal extension (CTE) of unknown function (Specht et al., 2011). To determine whether the NTD and/or CTE regions

(D) Loss of Cue5 blocks the autophagic transport of inactivated 26S proteasomes to the vacuole. Cells as described in (A) were visualized by confocal fluorescence microscopy 8 hr after transfer from +N medium to –N or +MG132 (80 μM) media. Shown are the fluorescence (GFP) images only. N, nucleus; V, vacuole; ? identifies cytoplasmic puncta similar to IPOD structures. Scale bar, 2 μm.

(E) Quantification of the cellular distribution of 26S proteasomes as visualized in (D). Cells were treated with or without N starvation or 80 μM MG132 for 8 hr. Each bar represents analysis of at least 200 cells.

See also Figures S5 and S6.

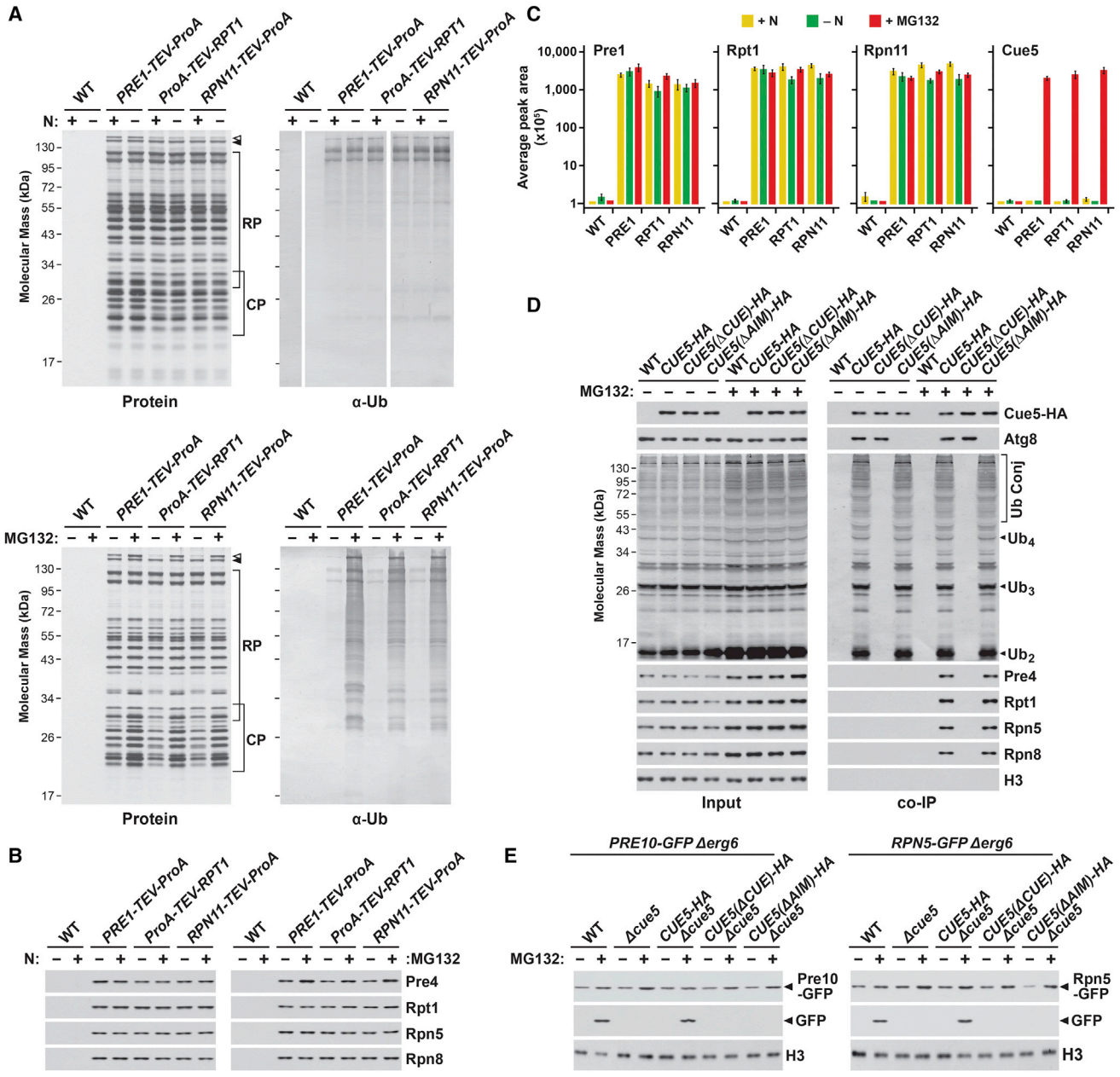

Figure 6. 26S Proteasome Inactivation by MG132 Triggers Extensive Ubiquitylation of the Particle and Association of Cue5

(A) Inactivated 26S proteasomes are ubiquitylated. *PRE1-TEV-ProA*, *ProA-TEV-RPT1*, and *RPN11-TEV-ProA* cells with or without the Δ*erg6* mutation were grown on +N medium or switched to –N or +MG132 (80 μM) media for 8 hr, before affinity enrichment of 26S proteasomes based on the ProA tag. The purified particles were subjected to SDS-PAGE and either stained for protein with silver (left panels) or probed by immunoblotting with anti-ubiquitin (Ub) antibodies (right panels). Top panels: 26S proteasomes purified from N-starved cells. Bottom panels: 26S proteasomes purified from MG132-treated cells. The immunoblot in the top panel was over-exposed relative to the bottom panel to accentuate the anti-ubiquitin antibody signal for proteasomes from N-starved cells. The distributions of CP and RP subunits are indicated by the brackets. Open and closed arrowheads locate Blm10 and Ecm29, respectively.

(B) Relative abundance of various 26S proteasome subunits in the preparations described in (A). Equal amounts of proteasomes were subjected to immunoblot analysis with antibodies specific for the indicated CP (Pre4) and RP (Rpt1, Rpn5, and Rpn8) subunits.

(C) 26S proteasomes purified from MG132-treated cells are enriched for Cue5. The preparations from (A) were subjected to tandem mass spectrometry followed by label-free quantification of the CP subunit Pre1, the RP subunits Rpt1 and Rpn11, and Cue5, based on peptide peak areas. Each bar represents the average of two technical replicates (±SD).

(D) Atg8 and Cue5 form a complex with ubiquitylated 26S proteasomes. Δ*erg6* cells expressing *CUE5-HA* or mutants missing either the ubiquitin-binding CUE domain or the AIM sequence were incubated for 8 hr with or without 80 μM MG132. Cue5-HA or mutant forms were then immunoprecipitated from lysed cells with anti-HA antibody beads. Input and bound proteins were visualized by immunoblot analysis with anti-HA, anti-Atg8 and anti-ubiquitin antibodies, plus antibodies

(legend continued on next page)

are required for MG132-induced proteaphagy, we used the GFP cleavage of Pre10-GFP and Rpn5-GFP to test Δ*hsp42* strains complemented with HA-tagged Hsp42 (Hsp42-HA) or versions with the NTD or CTE deleted (Hsp42(ΔNTD)-HA and Hsp42(ΔCTE)-HA, respectively). Whereas the CTE deletion performed like wild-type Hsp42, the NTD deletion could not restore the release of free GFP to the Δ*hsp42* background, thus implicating the NTD specifically in the autophagic clearance of inactivated 26S proteasomes (Figure 7B).

When the cellular dynamics of MG132-inactivated proteasomes were tracked in the Δ*hsp42* mutant by confocal fluorescence microscopy of the Pre10-GFP and Rpn5-GFP reporters, a noticeably different pattern was observed as compared to those in wild-type and the autophagy mutants. Instead of the fluorescence accumulating in vacuoles like wild-type, or coalescing into bright cytoplasmic foci as in the Δ*atg7*, Δ*atg10*, and Δ*cue5* backgrounds, the GFP signal either remained in the nucleus or became diffuse within the cytoplasm in the Δ*hsp42* cells (Figures 7C and 7D). Taken together, it appears that Hsp42 acts upstream of Cue5-mediated proteaphagy, possibly by helping coalesce inactive particles within the IPOD, either before or after their ubiquitylation. To provide a further connection between proteaphagy and IPOD, we attempted to co-localize Pre10-GFP with the IPOD marker Rnq1-mCherry (Kaganovich et al., 2008) in cells stimulated for proteaphagy with MG132. As shown in Figure 7D, we could identify cytoplasmic foci simultaneously containing both reporters soon after exposing the cells to MG132 (4 hr), strongly suggesting that these foci were indeed IPOD structures also containing dysfunctional 26S proteasomes.

Alternatively, it was possible that the proteasome aggregates seen with the Pre10-GFP and Rpn5-GFP reporters upon short exposures to MG132 actually reflect particles becoming concentrated into the cytoplasmic PAS foci that precede autophagosome formation. To test this possibly, we examined proteaphagy in cells lacking components of the Atg1 kinase complex (Δ*atg1*, Δ*atg11*, Δ*atg13*, and Δ*atg17*), which plays a crucial role scaffolding the PAS (Reggiori and Klionsky, 2013). As shown in Figure 7E, the 26S proteasome aggregates that appear soon after MG132 treatment were still evident in these mutant backgrounds, suggesting that they are not PAS-related.

DISCUSSION

The levels and activity of the 26S proteasome are controlled at multiple levels, including activation of the associated transcriptional regulon that responds to proteolytic demand, assembly through dedicated chaperones, interchange of subunit isoforms with unique activities, various post-translational modifications, alterations in CP/RP affinity, and sequestration of excess particles (Schmidt and Finley, 2014). Together with our prior studies in *Arabidopsis* (Marshall et al., 2015) and a recent report by Waite et al. (2016) in yeast, we show here that autophagy provides an additional control point that eliminates excess or damaged proteasomes.

As in *Arabidopsis*, two proteaphagic routes operate in yeast, one responsive to nitrogen availability that works through the Atg1 kinase and presumably upstream nutrient sensors such as Tor1/2 (Reggiori and Klionsky, 2013) and a second route that detects and removes inactive or dysfunctional particles. Both routes converge on the core autophagy machinery that includes the conjugation cascade that lipidates Atg8, the Atg9 complex that delivers membranes to the expanding phagophore and the PI3K complex that decorates the autophagic membranes with PI3P (Reggiori and Klionsky, 2013). While the first two complexes are essential for proteaphagy during both nitrogen starvation and proteasome inactivation, deletion of the PI3K complex does not completely block turnover, suggesting that modification of the membranes with PI3P is important but not required. Our findings with yeast largely agree with the more limited analyses by Waite et al., (2016), with the sole exception being the role of Atg11, which they found was not required for starvation-induced proteaphagy, but which we found is essential, along with the other components of the Atg1 complex.

Emerging data indicate that much of selective autophagy is directed by a suite of receptors that dock specific cargo to Atg8-PE lining the expanding phagophore. We previously implicated the RP subunit RPN10 as the *Arabidopsis* receptor for clearing dysfunctional 26S proteasomes (Marshall et al., 2015). RPN10 binds ATG8 through an AIM sequence and to proteasomes that become extensively ubiquitylated after inactivation via a UIM with high affinity for poly-ubiquitin chains. Surprisingly, whereas yeast also extensively ubiquitylates 26S proteasomes upon inactivation, this fungus instead employs the evolutionary unrelated autophagic receptor Cue5 (Lu et al., 2014), which contains an AIM fused to the distinct ubiquitin-binding CUE motif. The lack of affinity of yeast Rpn10 for Atg8, combined with normal proteasome turnover upon MG132 inhibition in *Δrpn10* strains, ruled out a role for this receptor in yeast proteaphagy. Instead, a direct role for Cue5 was demonstrated by the ability of the *Δcue5* mutant to block MG132-induced proteaphagy, roles for both the CUE and AIM sequences in this clearance, the ability of Cue5 to simultaneously bind Atg8 and ubiquitylated 26S proteasomes, and by the dramatically increased association of Cue5 with inactivated particles through the attached ubiquitin moieties.

against various 26S proteasome subunits. Immunoblotting with anti-histone H3 antibodies was included as a control. High molecular mass ubiquitin conjugates and poly-ubiquitin chains containing two, three, and four monomers are highlighted by the bracket and arrowheads, respectively.

(E) Cue5 mutants missing either the CUE domain or the AIM sequence cannot direct MG132-induced proteaphagy. *CUE5-HA* or the *CUE5-(ΔCUE)-HA* and *CUE5-(ΔAIM)-HA* mutations were introduced into *PRE10-GFP* Δ*cue5* Δ*erg6* or *RPN5-GFP* Δ*cue5* Δ*erg6* cells. The cells were grown in +N medium, switched to +MG132 (80 μM) medium for 8 hr, and then assayed for the release of free GFP by immunoblot analysis of total cell extracts with anti-GFP antibodies, as in Figure 2. Only portions of the gel containing the GFP fusions or free GFP are shown. Immunodetection of histone H3 was included to confirm near equal protein loading.

See also Figure S7.

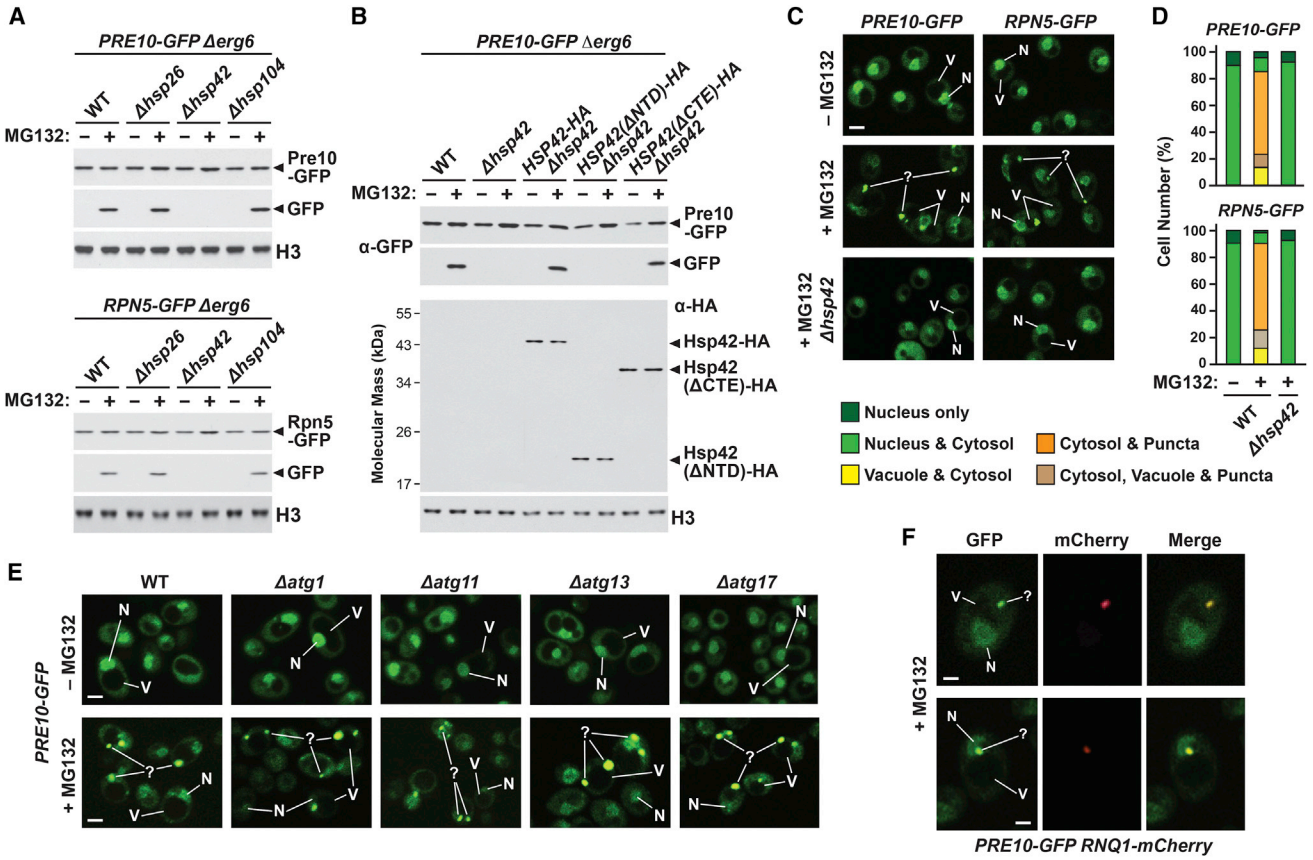

Figure 7. Hsp42 Is Required for MG132-Induced Proteaphagy, Possibly by Mediating Its Aggregation into IPOD Structures

(A) Hsp42, but not Hsp26 or Hsp104, is required for MG132-induced proteaphagy. Mutations deleting the indicated heat shock proteins were introduced into *PRE10-GFP* Δ*erg6* or *RPN5-GFP* Δ*erg6* backgrounds. Cells grown on +N medium were switched to +MG132 (80 μM) medium for 8 hr, and then assayed for the release of free GFP by immunoblot analysis of total cell extracts with anti-GFP antibodies, as in Figure 2. Only portions of the gel containing the GFP fusions or free GFP are shown. Immunodetection of histone H3 was included to confirm near equal protein loading.

(B) The N-terminal domain (NTD) of Hsp42 is required for MG132-induced proteaphagy. *HSP42-HA* or the *HSP42(ΔNTD)-HA* and *HSP42(ΔCTE)-HA* mutations were introduced into *PRE10-GFP* Δ*hsp42* Δ*erg6* cells. The cells were grown in +N medium, switched to +MG132 (80 μM) medium for 8 hr, and then assayed for the release of free GFP by immunoblot analysis of total cell extracts with anti-GFP antibodies, as in (A). Only portions of the gel containing the GFP fusions or free GFP are shown (top two panels). The third panel shows the expression levels of the Hsp42-HA, Hsp42(ΔNTD)-HA, and Hsp-42(ΔCTE)-HA proteins, as detected with anti-HA antibodies. Immunodetection of histone H3 was included to confirm near equal protein loading.

(C) Hsp42 is required for the formation of cytosolic proteasome aggregates upon MG132 treatment. The cells described in (A) were visualized by confocal fluorescence microscopy 4 hr after transfer from +N to +MG132 (80 μM) medium. Shown are the fluorescence (GFP) images only. N, nucleus; V, vacuole; ? identifies cytoplasmic puncta similar to IPOD structures (also applies in E and F). Scale bar, 2 μm.

(D) Quantification of the cellular distribution of 26S proteasomes as visualized in (C). Cells were treated with or without 80 μM MG132 for 8 hr. Each bar represents analysis of at least 180 cells.

(E) The Atg1 kinase complex is not required for proteasome aggregation. Shown are representative wild-type, Δ*atg1*, Δ*atg11*, Δ*atg13*, or Δ*atg17* cells expressing *PRE10-GFP* with the Δ*erg6* mutation, as visualized by confocal fluorescence microscopy 4 hr after transfer from +N medium to +MG132 (80 μM) medium. Shown are the fluorescence (GFP) images only. Scale bar, 2 μm.

(F) The IPOD-like structures containing Pre10-GFP that are formed early during MG132 exposure also contain the IPOD marker Rnq1-mCherry. *PRE10-GFP RNQ1-mCherry* Δ*erg6* cells treated for 4 hr with 80 μM MG132 were visualized by confocal fluorescence microscopy as in (C). Shown are the GFP, mCherry, and merged images only. Scale bar, 1 μm.

Among yeast proteins with ubiquitin-binding CUE domains, only Cue5 interacts with Atg8 and participates in the proteaphagy of dysfunctional 26S proteasomes, thus demonstrating a specific role for this family member. That yeast Cue5 and *Arabidopsis* RPN10 fulfill identical functions in two different kingdoms despite employing dissimilar AIM (WQPL versus LLDQA) and ubiquitin-binding motifs (CUE versus UIM) provide an excellent example of convergent evolution of a process starting with different building blocks. The increased binding of Cue5 to inactivated proteasomes, and its reduced binding upon ubiquitin removal with USP2, is reminiscent of that seen with *Arabidopsis* RPN10, where its proteasome occupancy substantially increases upon inactivation by binding to the attached ubiquitins (Marshall et al., 2015).

Previous studies were consistent with metazoans also utilizing proteaphagy to clear inactive proteasomes (Cuervo et al., 1995;

Dengjel et al., 2012). In humans, we anticipate that the Cue5 ortholog Tollip is involved, given its role in removing ubiquitylated cytoplasmic substrates in addition to roles in endocytosis and innate immunity (Lu et al., 2014) and our observations using Y2H that the human ortholog of *Arabidopsis* RPN10 (PSMD4) does not bind the Atg8 orthologs MAP1LC3a or GABARAP (Figure S5B). However, we note that other ubiquitin-binding autophagic receptors could also be candidates in humans, including p62/SQSTM1, NBR1, optineurin, NDP52, or TAX1BP1 (Khaminets et al., 2016; Rogov et al., 2014).

At present, the identity of the proteaphagy receptor during nitrogen stress is unknown (Waite et al., 2016; this study). One possibility is that no receptor is required, and 26S proteasome clearance during nitrogen starvation is driven by a bulk, nonselective process that indiscriminately engulfs cytoplasmic material. In support of this, we found that the rate of yeast proteaphagy during nitrogen starvation roughly mirrors that for bulk protein loss (see Figure S1B). Arguing against bulk proteaphagy, however, is the observation that starvation-induced turnover of the CP, but not the RP, in yeast depends on the deubiquitylating enzyme Ubp3, indicating a specific role for ubiquitin in this process (Waite et al., 2016). We also tested here a number of known autophagic receptors besides Cue5 (Atg19, Atg32, Atg34, Atg36, Atg39, and Atg40), none of which appear to be involved (Figure 4A). One failure of particular note is Atg39, which participates in nucleophagy, i.e., autophagy of nuclear components (Mochida et al., 2015). Given that most 26S proteasomes are in the nucleus, while autophagic engulfment and vacuolar transport happen in the cytoplasm, a mechanism should exist for the nuclear export of unwanted or damaged 26S proteasomes during both nitrogen starvation- and MG132-induced proteaphagy that might have involved this receptor. Furthermore, piecemeal microautophagy of the nucleus, which depends on the nuclear envelope receptor Nvj1, also does not appear to have a role in proteaphagy (Waite et al., 2016).

A key question in the proteaphagy of inactivated proteasomes is how cells can discriminate between active and dysfunctional particles and trigger ubiquitylation of the latter. It is also unclear which subunits are modified and at what sites and the identities of the responsible E3 ubiquitin ligase(s). Numerous proteomic studies have detected ubiquitylated proteasome subunits (e.g., Besche et al., 2014; Book et al., 2010; Kim et al., 2011, 2013), but their connection to proteaphagy, if any, awaits. Likewise, several E3s are known to associate with 26S proteasomes (Crosas et al., 2006; Xie and Varshavsky, 2000), some of which appear to ubiquitylate specific subunits (Besche et al., 2014), but their function(s) remain to be determined.

Our studies with MG132 demonstrate that inhibition of CP peptidase activity stimulates autophagy of both the CP and RP at indistinguishable rates, implying that both sub-complexes are degraded together, possibly via a common ubiquitylation signal. However, our follow-up studies with genetically compromised particles (the *doa5-1* allele of Pup2 [α_5] and *rpn5*Δ*C*) showed that the CP and RP can be degraded separately, using both Cue5 and the core autophagic machinery. Together, the data imply that compromised CP and RP can be separately detected, and likely ubiquitylated, before clearance via a Cue5-dependent mechanism. These results are consistent with those of Waite et al. (2016), who reported that the CP and RP are degraded by separate pathways in response to nitrogen starvation. One possible regulator for proteaphagy of compromised CP and/or RP is Ecm29, which mediates a quality control checkpoint prior to CP-RP assembly (Lehmann et al., 2010). Ecm29 promotes assembly of the 26S proteasome in conjunction with the E3 Not4 (Panasenko and Collart, 2011) and associates to a greater extent when the CP-RP interface is impaired by mutation (Park et al., 2011). Notably, a tighter association of the CP and RP have been observed upon inhibition of the CP (Kleijnen et al., 2007), thus potentially explaining why both subcomplexes are removed following MG132 exposure, even though only the CP active sites are compromised.

Besides autophagic transport of 26S proteasomes to the vacuole for breakdown, dynamic re-localization of these particles to other cytoplasmic features has been observed, including PSG and IPOD structures (Laporte et al., 2008; Peters et al., 2015, 2016; Weberruss et al., 2013). PSGs form during carbon starvation and represent cytoplasmic reservoirs of apparently active particles that reversibly aggregate when proteolytic demand is low and disperse when the cells are returned to carbon-rich media. Most of the proteasomes stored in PSGs presumably come from the nucleus, implying that a mechanism exists for both their export and resorption (Weberruss et al., 2013). In contrast, IPOD structures are peri-vacuolar foci proposed to provide a cytoprotective compartment that coalesces damaged/misfolded proteins from the rest of the cytoplasmic milieu as part of a protein quality control mechanism (Kaganovich et al., 2008; Miller et al., 2015). Such sequestration minimizes the toxic effects of such aggregates, as well as facilitating their disposal, some of which occurs via autophagy.

A key factor in IPOD assembly is Hsp42, an oligomeric chaperone that helps accumulate misfolded/insoluble proteins (Malinovska et al., 2012; Specht et al., 2011). Here, we found that Hsp42 is also essential for the selective proteaphagy of dysfunctional 26S proteasomes. This role of Hsp42, combined with the discovery that the inactivated particles accumulate in cytoplasmic foci also containing the IPOD marker Rnq1-mCherry, strongly suggest that IPOD represents an intermediate compartment before autophagic clearance. When Hsp42 and IPOD become engaged in proteaphagy, and their role(s) in proteasome ubiquitylation, are not yet clear. Whereas the loss of Cue5 and central components of the Atg8-mediated autophagy system still allow cytoplasmic aggregation of inactivated 26S proteasomes, loss of Hsp42 seems to prevent this aggregation, suggesting that Hsp42 and IPOD work upstream of Cue5 and autophagic engulfment. One possibility is that Hsp42 helps accumulate dysfunctional proteasome aggregates into IPOD foci after ubiquitin addition, while an alternative is that Hsp42 delivers dysfunctional proteasomes to IPOD, which then encourages their ubiquitylation through one or more associated E3s. Cue5 would then deliver the aggregated and ubiquitylated proteasomes to Atg8 lining the phagophore.

In conclusion, we provide further clarity regarding the interplay between the 26S proteasome and autophagy in eukaryotes and possible connections between IPOD-type compartments involving Hsp42 and proteasome homeostasis. Combined with prior studies (Marshall et al., 2015; Waite et al., 2016), our data

here support a conserved role for autophagy in controlling proteasome abundance through the ubiquitylation of dysfunctional particles, followed by their association with autophagic receptors such as RPN10 and Cue5 that simultaneously recognize the bound ubiquitin moieties and Atg8 lining the engulfing autophagic membranes. Taken together, the interplay between ubiquitin, proteaphagy, and IPOD provides an excellent paradigm for defining the protein quality control processes that mitigate the cytotoxic effects of aberrant/misfolded protein aggregates, which are at the core of many aggregation-prone pathologies (Kaganovich et al., 2008; Lu et al., 2014).

EXPERIMENTAL PROCEDURES

Yeast Strains and Manipulations

Unless otherwise stated, all yeast manipulations were performed according to standard protocols (Dunham et al., 2015). Details of all strains used in this study are given in Table S1. Cultures were grown overnight in YPDA medium at 30°C with vigorous shaking, diluted to an OD_{600} of 0.1 in 15 ml, then grown for an additional 2–3 hr until an OD_{600} of ~0.5 was reached. Aliquots of cells corresponding to 1.5 OD units were then taken at the indicated times. For nitrogen starvation experiments, cells were re-suspended in synthetic dropout medium lacking nitrogen (0.17% yeast nitrogen base without amino acids and ammonium sulfate, 2% glucose). For treatment with the proteasome inhibitor MG132, cells harboring the Δ*erg6* deletion (Lee and Goldberg, 1996) were grown in YPDA medium as above, followed by addition of 80 μM MG132 for the indicated times. Further details of all methods are given in the Supplemental Experimental Procedures and Tables S2 and S3.

Confocal Fluorescence Microscopy

Cells grown and treated as above were immobilized onto concanavalin A-coated slides and visualized with a Nikon A1 super-resolution microscope. Excitation was performed at 488 or 543 nm, and emission was collected between 500 and 530 or 565 and 615 nm, for GFP and mCherry channels, respectively.

Quantitative Real-Time PCR Analysis

The cell walls of ~2×10^7 freshly harvested WT, Δ*erg6*, or Δ*erg6* Δ*rpn4* cells treated with or without MG132 were digested with 100 U of lyticase, and total RNA was then extracted using the RNeasy mini kit (QIAGEN) and converted into cDNA using the SuperScript III first-strand synthesis system (Invitrogen) and oligo$(dT)_{20}$ primers. PCR was performed with LightCycler 480 SYBR Green I master mix and the relative transcript abundance of target genes was determined using the comparative threshold cycle method (Pfaffl, 2001), with *ALG9* and *TFC1* used as internal reference standards.

Pho8Δ60 Enzyme Assay

The Pho8Δ60 assay for quantitative measurement of autophagic flux was performed essentially as previously described (Noda and Klionsky, 2008), using a spectrophotometric assay to monitor production of *p*-nitrophenol from *p*-nitrophenyl phosphate by measuring its absorbance at 400 nm.

Yeast Two-Hybrid Assays

Assays for protein-protein interactions were performed using the ProQuest two-hybrid system (Life Technologies). Pairwise gene combinations in pDEST22 and pDEST32 (or the empty vector controls) were co-transformed into strain MaV203. Interactions were identified by growth for 2 days at 30°C on synthetic complete medium lacking leucine, tryptophan, and histidine and containing 25 mM 3-amino-1,2,4-triazole.

Co-immunoprecipitation

Cells expressing wild-type or mutant versions of Cue5-HA were grown as above and treated with or without 80 μM MG132. Cells were lysed by vortexing in the presence of acid-washed glass beads, and clarified extract was incubated for 2 hr at 4°C with 50 μl EZview red anti-HA affinity gel (Sigma-Aldrich). The beads were collected by centrifugation at 6,000 × *g*, washed five times with ice-cold lysis buffer, and bound proteins were eluted by heating at 95°C for 5 min in SDS-PAGE sample buffer.

Proteasome Affinity Purifications

Purification of the 26S proteasome was performed essentially as previously described (Leggett et al., 2005), with minor modifications. Briefly, yeast strains were grown in 500 ml YPDA medium, treated with or without nitrogen starvation or 80 μM MG132, harvested, frozen in liquid nitrogen, ground to a fine powder, and rehydrated in 1 vol lysis buffer; proteins were then extracted on ice for 20 min. Following clarification, the supernatant was incubated for 2 hr at 4°C with 100 μl of rabbit whole molecule IgG antigen affinity gel (MP Biomedicals). The beads were washed with low or high salt buffers, treated with the deubiquitylating enzyme USP2 (Boston Biochem) where indicated, and bound protein was eluted by incubation for 1 hr at 30°C with 20 ng/μl of recombinant 6His-TEV protease in a total volume of 300 μl.

Tandem Mass Spectrometry

Approximately 30 μg of purified 26S proteasomes from each preparation performed as above were denatured in 6 M urea in a total volume of 300 μl, reduced with 10 mM DTT and then alkylated with 50 mM 2-chloro-2-iodoacetamide. Samples were diluted with 1.2 ml of 25 mM $(NH_4)HCO_3$ and then digested for 18 hr at 37°C with 1 μg sequencing grade trypsin (Promega). The resulting peptides were acidified with 10% trifluoroacetic acid, desalted on a 100 μl Bond Elut OMIX C18 pipette tip (Agilent Technologies), and resuspended in 60 μl of 5% acetonitrile, 0.1% formic acid. Peptides were separated by nano-scale liquid chromatography on a Dionex Ultimate 3000 Rapid Separation LC system (Thermo Scientific), with a 75 μm × 15 cm Acclaim PepMap RSLC C18 column (Thermo Scientific) and a 2 hr linear gradient from 3% to 44% acetonitrile in 0.1% formic acid. Peptides were then identified on-line with a Q Exactive Plus orbitrap mass spectrometer equipped with a Nanospray Flex ion source (both from Thermo Scientific). Full details of acquisition parameters and subsequent data analysis are given in the Supplemental Experimental Procedures. Briefly, the MS/MS spectra were analyzed using Proteome Discoverer software (Thermo Scientific) with a 1% false discovery rate, and label-free quantification was performed based on the universal signal response factor (Silva et al., 2006) using a minimum Quan value threshold of 0.0001 for unique peptides and "3 Top N" peptides for area calculation.

Phylogenetic and Statistical Analyses

The predicted amino acid sequences for all nine yeast CUE domains were aligned using Clustal Omega (http://www.clustal.org/omega) and then subjected to Bayesian phylogenetic analysis with MrBayes version 3.2 (Ronquist and Huelsenbeck, 2003). Quantified immunoblots and other datasets were statistically analyzed by ANOVA followed by Tukey's post hoc tests to identify significantly different data points.

SUPPLEMENTAL INFORMATION

Supplemental Information includes Supplemental Experimental Procedures, seven figures, and three tables and can be found with this article online at http://dx.doi.org/10.1016/j.celrep.2016.07.015.

AUTHOR CONTRIBUTIONS

R.S.M. and R.D.V. designed the project, analyzed all data, and wrote the manuscript. R.S.M. performed most of the experimental work. F.M. assisted with the mass spectrometry.

ACKNOWLEDGMENTS

The authors wish to thank Shay Ben-Aroya, E. Sethe Burgie, Katie J. Clowers, Daniel Finley, Mark Hochstrasser, Stefan Jentsch, Daniel J. Klionsky, and Susan Lindquist for sharing various yeast strains, antibodies, and other reagents. Dianne M. Duncan and Sarah J. Swanson helped with confocal microscopy. Robert C. Augustine, David C. Gemperline, Faqiang Li, and Joseph M. Walker

provided valuable advice and technical assistance. This work and R.S.M. were supported by the U.S. Department of Energy Office of Science; Office of Basic Energy Science; Chemical Sciences, Geosciences and Biosciences Division (DE-FG02-88ER13968). F.M. was supported by the U.S. National Science Foundation, Plant Genome Research Program (IOS-1339325).

Received: February 22, 2016
Revised: May 23, 2016
Accepted: July 3, 2016
Published: July 28, 2016

REFERENCES

Bajorek, M., Finley, D., and Glickman, M.H. (2003). Proteasome disassembly and downregulation is correlated with viability during stationary phase. Curr. Biol. *13*, 1140–1144.

Besche, H.C., Sha, Z., Kukushkin, N.V., Peth, A., Hock, E.M., Kim, W., Gygi, S., Gutierrez, J.A., Liao, H., Dick, L., and Goldberg, A.L. (2014). Autoubiquitination of the 26S proteasome on Rpn13 regulates breakdown of ubiquitin conjugates. EMBO J. *33*, 1159–1176.

Bhattacharyya, S., Yu, H., Mim, C., and Matouschek, A. (2014). Regulated protein turnover: snapshots of the proteasome in action. Nat. Rev. Mol. Cell Biol. *15*, 122–133.

Book, A.J., Gladman, N.P., Lee, S.S., Scalf, M., Smith, L.M., and Vierstra, R.D. (2010). Affinity purification of the *Arabidopsis* 26 S proteasome reveals a diverse array of plant proteolytic complexes. J. Biol. Chem. *285*, 25554–25569.

Chen, P., and Hochstrasser, M. (1995). Biogenesis, structure and function of the yeast 20S proteasome. EMBO J. *14*, 2620–2630.

Crosas, B., Hanna, J., Kirkpatrick, D.S., Zhang, D.P., Tone, Y., Hathaway, N.A., Buecker, C., Leggett, D.S., Schmidt, M., King, R.W., et al. (2006). Ubiquitin chains are remodeled at the proteasome by opposing ubiquitin ligase and deubiquitinating activities. Cell *127*, 1401–1413.

Cuervo, A.M., Palmer, A., Rivett, A.J., and Knecht, E. (1995). Degradation of proteasomes by lysosomes in rat liver. Eur. J. Biochem. *227*, 792–800.

Dengjel, J., Høyer-Hansen, M., Nielsen, M.O., Eisenberg, T., Harder, L.M., Schandorff, S., Farkas, T., Kirkegaard, T., Becker, A.C., Schroeder, S., et al. (2012). Identification of autophagosome-associated proteins and regulators by quantitative proteomic analysis and genetic screens. Mol. Cell. Proteomics *11*, 014035.

Dunham, M.J., Gartenberg, M.R., and Brown, G.W. (2015). Methods in Yeast Genetics and Genomics (Cold Spring Harbor Laboratory Press), pp. 1–256.

Farmer, L.M., Book, A.J., Lee, K.H., Lin, Y.L., Fu, H., and Vierstra, R.D. (2010). The RAD23 family provides an essential connection between the 26S proteasome and ubiquitylated proteins in *Arabidopsis*. Plant Cell *22*, 124–142.

Fatimababy, A.S., Lin, Y.L., Usharani, R., Radjacommare, R., Wang, H.T., Tsai, H.L., Lee, Y., and Fu, H. (2010). Cross-species divergence of the major recognition pathways of ubiquitylated substrates for ubiquitin/26S proteasome-mediated proteolysis. FEBS J. *277*, 796–816.

Finley, D. (2009). Recognition and processing of ubiquitin-protein conjugates by the proteasome. Annu. Rev. Biochem. *78*, 477–513.

Finley, D., Chen, X., and Walters, K.J. (2016). Gates, channels, and switches: elements of the proteasome machine. Trends Biochem. Sci. *41*, 77–93.

Fujiwara, T., Tanaka, K., Orino, E., Yoshimura, T., Kumatori, A., Tamura, T., Chung, C.H., Nakai, T., Yamaguchi, K., Shin, S., et al. (1990). Proteasomes are essential for yeast proliferation. cDNA cloning and gene disruption of two major subunits. J. Biol. Chem. *265*, 16604–16613.

Gladman, N.P., Marshall, R.S., Lee, K.H., and Vierstra, R.D. (2016). The proteasome stress regulon is controlled by a pair of NAC transcription factors in *Arabidopsis*. Plant Cell *28*, 1279–1296.

Haslbeck, M., Ignatiou, A., Saibil, H., Helmich, S., Frenzl, E., Stromer, T., and Buchner, J. (2004). A domain in the N-terminal part of Hsp26 is essential for chaperone function and oligomerization. J. Mol. Biol. *343*, 445–455.

Kaganovich, D., Kopito, R., and Frydman, J. (2008). Misfolded proteins partition between two distinct quality control compartments. Nature *454*, 1088–1095.

Kang, R.S., Daniels, C.M., Francis, S.A., Shih, S.C., Salerno, W.J., Hicke, L., and Radhakrishnan, I. (2003). Solution structure of a CUE-ubiquitin complex reveals a conserved mode of ubiquitin binding. Cell *113*, 621–630.

Khaminets, A., Behl, C., and Dikic, I. (2016). Ubiquitin-dependent and independent signals in selective autophagy. Trends Cell Biol. *26*, 6–16.

Kim, W., Bennett, E.J., Huttlin, E.L., Guo, A., Li, J., Possemato, A., Sowa, M.E., Rad, R., Rush, J., Comb, M.J., et al. (2011). Systematic and quantitative assessment of the ubiquitin-modified proteome. Mol. Cell *44*, 325–340.

Kim, D.Y., Scalf, M., Smith, L.M., and Vierstra, R.D. (2013). Advanced proteomic analyses yield a deep catalog of ubiquitylation targets in *Arabidopsis*. Plant Cell *25*, 1523–1540.

Kleijnen, M.F., Roelofs, J., Park, S., Hathaway, N.A., Glickman, M., King, R.W., and Finley, D. (2007). Stability of the proteasome can be regulated allosterically through engagement of its proteolytic active sites. Nat. Struct. Mol. Biol. *14*, 1180–1188.

Klionsky, D.J., and Schulman, B.A. (2014). Dynamic regulation of macroautophagy by distinctive ubiquitin-like proteins. Nat. Struct. Mol. Biol. *21*, 336–345.

Klionsky, D.J., Abdelmohsen, K., Abe, A., Abedin, M.J., Abeliovich, H., Acevedo Arozena, A., Adachi, H., Adams, C.M., Adams, P.D., Adeli, K., et al. (2016). Guidelines for the use and interpretation of assays for monitoring autophagy (3rd edition). Autophagy *12*, 1–222.

Lamb, C.A., Yoshimori, T., and Tooze, S.A. (2013). The autophagosome: origins unknown, biogenesis complex. Nat. Rev. Mol. Cell Biol. *14*, 759–774.

Laporte, D., Salin, B., Daignan-Fornier, B., and Sagot, I. (2008). Reversible cytoplasmic localization of the proteasome in quiescent yeast cells. J. Cell Biol. *181*, 737–745.

Lazarou, M., Sliter, D.A., Kane, L.A., Sarraf, S.A., Wang, C., Burman, J.L., Sideris, D.P., Fogel, A.I., and Youle, R.J. (2015). The ubiquitin kinase PINK1 recruits autophagy receptors to induce mitophagy. Nature *524*, 309–314.

Lee, D.H., and Goldberg, A.L. (1996). Selective inhibitors of the proteasome-dependent and vacuolar pathways of protein degradation in *Saccharomyces cerevisiae*. J. Biol. Chem. *271*, 27280–27284.

Leggett, D.S., Hanna, J., Borodovsky, A., Crosas, B., Schmidt, M., Baker, R.T., Walz, T., Ploegh, H., and Finley, D. (2002). Multiple associated proteins regulate proteasome structure and function. Mol. Cell *10*, 495–507.

Leggett, D.S., Glickman, M.H., and Finley, D. (2005). Purification of proteasomes, proteasome subcomplexes, and proteasome-associated proteins from budding yeast. Methods Mol. Biol. *301*, 57–70.

Lehmann, A., Niewienda, A., Jechow, K., Janek, K., and Enenkel, C. (2010). Ecm29 fulfils quality control functions in proteasome assembly. Mol. Cell *38*, 879–888.

Liu, C., Apodaca, J., Davis, L.E., and Rao, H. (2007). Proteasome inhibition in wild-type yeast Saccharomyces cerevisiae cells. Biotechniques *42*, 158–162, 160, 162.

Livnat-Levanon, N., Kevei, É., Kleifeld, O., Krutauz, D., Segref, A., Rinaldi, T., Erpapazoglou, Z., Cohen, M., Reis, N., Hoppe, T., and Glickman, M.H. (2014). Reversible 26S proteasome disassembly upon mitochondrial stress. Cell Rep. *7*, 1371–1380.

Lu, K., Psakhye, I., and Jentsch, S. (2014). Autophagic clearance of polyQ proteins mediated by ubiquitin-Atg8 adaptors of the conserved CUET protein family. Cell *158*, 549–563.

Lu, Y., Lee, B.H., King, R.W., Finley, D., and Kirschner, M.W. (2015). Substrate degradation by the proteasome: a single-molecule kinetic analysis. Science *348*, 1250834.

Malinovska, L., Kroschwald, S., Munder, M.C., Richter, D., and Alberti, S. (2012). Molecular chaperones and stress-inducible protein-sorting factors coordinate the spatiotemporal distribution of protein aggregates. Mol. Biol. Cell *23*, 3041–3056.

Marshall, R.S., and Vierstra, R.D. (2015). Eat or be eaten: The autophagic plight of inactive 26S proteasomes. Autophagy *11*, 1927–1928.

Marshall, R.S., Li, F., Gemperline, D.C., Book, A.J., and Vierstra, R.D. (2015). Autophagic degradation of the 26S proteasome is mediated by the dual ATG8/ubiquitin receptor RPN10 in *Arabidopsis*. Mol. Cell *58*, 1053–1066.

Miller, S.B., Ho, C.T., Winkler, J., Khokhrina, M., Neuner, A., Mohamed, M.Y., Guilbride, D.L., Richter, K., Lisby, M., Schiebel, E., et al. (2015). Compartment-specific aggregases direct distinct nuclear and cytoplasmic aggregate deposition. EMBO J. *34*, 778–797.

Mochida, K., Oikawa, Y., Kimura, Y., Kirisako, H., Hirano, H., Ohsumi, Y., and Nakatogawa, H. (2015). Receptor-mediated selective autophagy degrades the endoplasmic reticulum and the nucleus. Nature *522*, 359–362.

Noda, T., and Klionsky, D.J. (2008). The quantitative Pho8Δ60 assay of nonspecific autophagy. Methods Enzymol. *451*, 33–42.

Panasenko, O.O., and Collart, M.A. (2011). Not4 E3 ligase contributes to proteasome assembly and functional integrity in part through Ecm29. Mol. Cell. Biol. *31*, 1610–1623.

Paraskevopoulos, K., Kriegenburg, F., Tatham, M.H., Rösner, H.I., Medina, B., Larsen, I.B., Brandstrup, R., Hardwick, K.G., Hay, R.T., Kragelund, B.B., et al. (2014). Dss1 is a 26S proteasome ubiquitin receptor. Mol. Cell *56*, 453–461.

Park, S., Kim, W., Tian, G., Gygi, S.P., and Finley, D. (2011). Structural defects in the regulatory particle-core particle interface of the proteasome induce a novel proteasome stress response. J. Biol. Chem. *286*, 36652–36666.

Peters, L.Z., Karmon, O., David-Kadoch, G., Hazan, R., Yu, T., Glickman, M.H., and Ben-Aroya, S. (2015). The protein quality control machinery regulates its misassembled proteasome subunits. PLoS Genet. *11*, e1005178.

Peters, L.Z., Karmon, O., Miodownik, S., and Ben-Aroya, S. (2016). Proteasome storage granules are transiently associated with the insoluble protein deposit (IPOD). J. Cell Sci. *129*, 1190–1197.

Peth, A., Uchiki, T., and Goldberg, A.L. (2010). ATP-dependent steps in the binding of ubiquitin conjugates to the 26S proteasome that commit to degradation. Mol. Cell *40*, 671–681.

Pfaffl, M.W. (2001). A new mathematical model for relative quantification in real-time RT-PCR. Nucleic Acids Res. *29*, e45.

Radhakrishnan, S.K., Lee, C.S., Young, P., Beskow, A., Chan, J.Y., and Deshaies, R.J. (2010). Transcription factor Nrf1 mediates the proteasome recovery pathway after proteasome inhibition in mammalian cells. Mol. Cell *38*, 17–28.

Reggiori, F., and Klionsky, D.J. (2013). Autophagic processes in yeast: mechanism, machinery and regulation. Genetics *194*, 341–361.

Rogov, V., Dötsch, V., Johansen, T., and Kirkin, V. (2014). Interactions between autophagy receptors and ubiquitin-like proteins form the molecular basis for selective autophagy. Mol. Cell *53*, 167–178.

Ronquist, F., and Huelsenbeck, J.P. (2003). MrBayes 3: Bayesian phylogenetic inference under mixed models. Bioinformatics *19*, 1572–1574.

Saito, A., Watanabe, T.K., Shimada, Y., Fujiwara, T., Slaughter, C.A., DeMartino, G.N., Tanahashi, N., and Tanaka, K. (1997). cDNA cloning and functional analysis of p44.5 and p55, two regulatory subunits of the 26S proteasome. Gene *203*, 241–250.

Schmidt, M., and Finley, D. (2014). Regulation of proteasome activity in health and disease. Biochim. Biophys. Acta *1843*, 13–25.

Sha, Z., and Goldberg, A.L. (2014). Proteasome-mediated processing of Nrf1 is essential for coordinate induction of all proteasome subunits and p97. Curr. Biol. *24*, 1573–1583.

Shi, Y., Chen, X., Elsasser, S., Stocks, B.B., Tian, G., Lee, B.H., Shi, Y., Zhang, N., de Poot, S.A., Tuebing, F., et al. (2016). Rpn1 provides adjacent receptor sites for substrate binding and deubiquitination by the proteasome. Science *351*, 831.

Shih, S.C., Prag, G., Francis, S.A., Sutanto, M.A., Hurley, J.H., and Hicke, L. (2003). A ubiquitin-binding motif required for intramolecular monoubiquitylation, the CUE domain. EMBO J. *22*, 1273–1281.

Sica, V., Galluzzi, L., Bravo-San Pedro, J.M., Izzo, V., Maiuri, M.C., and Kroemer, G. (2015). Organelle-specific initiation of autophagy. Mol. Cell *59*, 522–539.

Silva, J.C., Gorenstein, M.V., Li, G.Z., Vissers, J.P., and Geromanos, S.J. (2006). Absolute quantification of proteins by LCMSE: a virtue of parallel MS acquisition. Mol. Cell. Proteomics *5*, 144–156.

Specht, S., Miller, S.B., Mogk, A., and Bukau, B. (2011). Hsp42 is required for sequestration of protein aggregates into deposition sites in *Saccharomyces cerevisiae*. J. Cell Biol. *195*, 617–629.

Tomko, R.J., Jr., and Hochstrasser, M. (2013). Molecular architecture and assembly of the eukaryotic proteasome. Annu. Rev. Biochem. *82*, 415–445.

Waite, K.A., De-La Mota-Peynado, A., Vontz, G., and Roelofs, J. (2016). Starvation induces proteasome autophagy with different pathways for core and regulatory particles. J. Biol. Chem. *291*, 3239–3253.

Weberruss, M.H., Savulescu, A.F., Jando, J., Bissinger, T., Harel, A., Glickman, M.H., and Enenkel, C. (2013). Blm10 facilitates nuclear import of proteasome core particles. EMBO J. *32*, 2697–2707.

Wild, P., Farhan, H., McEwan, D.G., Wagner, S., Rogov, V.V., Brady, N.R., Richter, B., Korac, J., Waidmann, O., Choudhary, C., et al. (2011). Phosphorylation of the autophagy receptor optineurin restricts *Salmonella* growth. Science *333*, 228–233.

Woolford, C.A., Daniels, L.B., Park, F.J., Jones, E.W., Van Arsdell, J.N., and Innis, M.A. (1986). The *PEP4* gene encodes an aspartyl protease implicated in the posttranslational regulation of *Saccharomyces cerevisiae* vacuolar hydrolases. Mol. Cell. Biol. *6*, 2500–2510.

Xie, Y., and Varshavsky, A. (2000). Physical association of ubiquitin ligases and the 26S proteasome. Proc. Natl. Acad. Sci. USA *97*, 2497–2502.

Xie, Y., and Varshavsky, A. (2001). RPN4 is a ligand, substrate, and transcriptional regulator of the 26S proteasome: a negative feedback circuit. Proc. Natl. Acad. Sci. USA *98*, 3056–3061.